https://doi.org/10.5194/egusphere-2026-6664
Preprint. Discussion started: 22 November 2026
© Author(s) 2026. CC BY 4.0 License.

VISIT-4type v1.0: Forest age structure, wood harvest and land-cover transitions in a dynamic global vegetation model

Jianyong Dong[1,2], Shuting Zhao[2], Ximing Chen[1], Zhangcai Yin[1], Akihiko Ito[2*]
[1]School of Resources and Environmental Engineering, Wuhan University of Technology, Wuhan, China, [2]Graduate School of Agricultural and Life Sciences, The University of Tokyo, Tokyo, Japan
Correspondence: Akihiko Ito (akihikoito@g.ecc.u-tokyo.ac.jp)

Abstract

In dynamic global vegetation models (DGVMs), representing land-use change solely through net changes in land-cover fractions can obscure forest disturbance histories and associated carbon transfers. Here we describe VISIT-4type (v1.0), which extends the two-type framework of the Vegetation Integrative SImulator for Trace gases (VISIT) to primary forest, secondary forest, cropland and other natural vegetation. Both forest types are resolved into six age cohorts; a transition ledger transfers carbon with changing area; wood harvest follows Land-Use Harmonization 2 (LUH2) area requests with separate fuelwood and industrial-wood pathways; and secondary-forest leaf traits are derived from the TRY database. Six model configurations under common environmental forcing are compared to quantify the contributions of these developments to differences in simulated net biome productivity (NBP) over 1850–2019. Against eddy-covariance observations, VISIT-4type reduced the per-site root-mean-square error (RMSE) of annual gross primary production (GPP), net ecosystem exchange (NEE) and ecosystem respiration at 64%, 74% and 74% of forest sites ($p \leq 0.015$); the median RMSE decreased from 615 to 565, 303 to 286 and 499 to 434 g C m^{-2} yr^{-1}, without significant changes in correlation. Against FLUXCOM X-BASE (2001–2019), the area-weighted mean RMSE of monthly GPP and NEE decreased by 0.42 and 0.25 g C m^{-2} $month^{-1}$, with lower errors over 46.7% and 56.1% of the evaluated land, concentrated in grid cells with a history of wood harvest or forest

https://doi.org/10.5194/egusphere-2026-6664
Preprint. Discussion started: 22 November 2026
© Author(s) 2026. CC BY 4.0 License.



clearing. Harvested stem carbon was 44–61% of LUH2 wood-harvest biomass, reflecting lower simulated carbon density in harvested primary forest and in the young secondary forests that dominate the harvest requests. Over 1850–2019, global mean NBP was 0.173 Pg C yr^{-1} lower in VISIT-4type than in VISIT-2type. Wood harvest with forest age structure accounted for −0.171 Pg C yr^{-1} of this difference, whereas land-cover structure and transitions contributed +0.026 Pg C yr^{-1} and secondary-forest traits −0.027 Pg C yr^{-1}. Relative to 1850, the 2019 ecosystem carbon-stock difference between the two versions (−81.2 Pg C) was about 52 Pg C more negative than the cumulative NBP difference over 1851–2019 (−29.2 Pg C). About 45 Pg C of this gap arises because abandoned cropland in VISIT-2type inherits the per-area carbon of natural vegetation without a corresponding uptake flux, which are not included in its ecosystem stock. These results show that disturbed-stand carbon density and the end use of harvested wood are key controls on simulated land-use effects, and that flux evaluation needs to be complemented by forest observations that resolve stand age and successional stage.

1 Introduction

Land-use change and forest management alter terrestrial carbon storage and exchange through vegetation removal, regrowth and the decomposition of residues and wood products (Hansis et al., 2015; Houghton and Nassikas, 2017). Forests play a central role by storing carbon and absorbing atmospheric CO_2 during recovery (Pan et al., 2011; Shevliakova et al., 2009). The net CO_2 flux associated with land-use change, denoted E_{LUC}, remains a major anthropogenic source and an uncertain component of the global carbon budget (Friedlingstein et al., 2026; Pongratz et al., 2014). In dynamic global vegetation models (DGVMs), the magnitude and timing of simulated E_{LUC} depend on the disturbance history and carbon density of affected vegetation, the fate of removed biomass, and subsequent vegetation and soil recovery (Dong et al., 2026).

https://doi.org/10.5194/egusphere-2026-6664
Preprint. Discussion started: 22 November 2026
© Author(s) 2026. CC BY 4.0 License.

Land-use schemes must therefore link changes in land-cover area to the associated disturbances, carbon transfers and regrowth.

Land-use carbon flux estimates remain uncertain because of differences in model process representation and carbon-accounting conventions (Friedlingstein et al., 2026; Grassi et al., 2023). Net changes in land-cover fractions do not uniquely identify the disturbance and recovery histories within a grid cell. Net area change records the balance between gains and losses of a land-cover type, whereas gross transitions retain the individual directional transfers, including opposing flows that cancel in the net change (Wilkenskjeld et al., 2014). The Land-Use Harmonization 2 (LUH2) dataset provides annual land-use fractions, gross transitions, secondary-land dynamics and wood-harvest information, although their translation into modelled land-cover change requires explicit implementation choices (Hurtt et al., 2020; Ma et al., 2020). For example, forest clearing can coincide with recovery on abandoned cropland, while wood harvest can replace mature stands with young regrowth without changing total forest area (Yue et al., 2018a; Yue et al., 2018b). Primary and secondary forests can differ in carbon density, and secondary-forest carbon accumulation depends on stand age and disturbance history (Poorter et al., 2016; Pugh et al., 2019). Consequently, identical net area changes can produce different carbon removals and subsequent fluxes. This is particularly relevant to area-driven harvest, for which carbon removal depends on the density and selection of simulated stands rather than harvested area alone.

Several DGVMs provide established approaches for representing forest disturbance and recovery. ORCHIDEE-MICT and CABLE incorporate forest age structure and disturbance or management processes (Haverd et al., 2018; Yue et al., 2018b). LPJ-GUESS couples forest management with cohort dynamics (Lindeskog et al., 2021), while LPJ-wsl v2.0 represents ecosystem age classes, gross transitions and harvested-wood pathways (Calle and Poulter, 2021). These approaches link disturbance histories to the carbon density of affected stands, biomass removal and subsequent regrowth. Their effects nevertheless depend on how they interact with each model's

https://doi.org/10.5194/egusphere-2026-6664
Preprint. Discussion started: 22 November 2026
© Author(s) 2026. CC BY 4.0 License.

physiological processes, carbon allocation and turnover. Extending these representations to another model therefore requires both their integration into its carbon-cycle framework and evaluation of the resulting changes in stocks and fluxes.

The Vegetation Integrative SImulator for Trace gases (VISIT) simulates terrestrial carbon cycling through photosynthesis, respiration, allocation, litterfall and decomposition (Ito, 2010; Ito, 2019). It has been used in regional and global assessments and has participated in ISIMIP and TRENDY intercomparisons (Friedlingstein et al., 2026; Frieler et al., 2024). In the configuration used here as the reference, VISIT represents cropland and natural vegetation as two land-cover types, without separate primary- and secondary-forest states or age cohorts, and does not include a wood-harvest scheme. This aggregation limits the representation of disturbance-specific carbon removal and forest recovery, motivating a framework that links forest states, area changes and carbon routing.

Beyond forest structure and disturbance history, secondary-forest physiology can also influence carbon exchange during recovery. Age cohorts represent differences in biomass and canopy development, but stand age alone does not specify the changes in community composition and leaf traits associated with secondary succession (Poorter et al., 2021). The TRY database provides plant-trait observations from which separate, biome-specific parameters for secondary forests can be derived (Kattge et al., 2020). Evaluating these parameters alongside changes in forest states, age cohorts and harvest allows us to determine how physiological adjustments affect simulated carbon fluxes and whether they improve agreement with observations.

Here we describe VISIT-4type, which distinguishes primary forest, secondary forest, cropland and other natural vegetation. The extension introduces six age cohorts for each forest type, a transition ledger linking area changes with carbon transfers, area-driven wood harvest with separate fuelwood and industrial-wood pathways, and TRY-derived secondary-forest leaf traits. Using six model configurations under common environmental forcing, we address four questions: (1) How does VISIT-4type perform

https://doi.org/10.5194/egusphere-2026-6664
Preprint. Discussion started: 22 November 2026
© Author(s) 2026. CC BY 4.0 License.

relative to VISIT-2type against site- and grid-scale carbon-flux benchmarks? (2) How does simulated harvested stem carbon compare with LUH2 wood-harvest biomass under shared harvest-area forcing, and how is removed carbon partitioned? (3) How do land-cover structure and transitions, wood harvest including age structure, and secondary-forest traits contribute to differences in NBP and carbon stocks over 1850–2019? (4) How does the change in the ecosystem-carbon-stock contrast relative to 1850 compare with the cumulative NBP contrast over 1851–2019?

2 Model development

2.1 Four-type land-cover framework

We extended VISIT from two land-cover types, cropland and natural vegetation (Ito, 2010; Ito, 2019) , to four: primary forest (V0), secondary forest (V1), cropland (V2), and other natural vegetation, including pasture (V3). The original shared natural-vegetation state could not retain separate primary- and secondary-forest disturbance histories or carbon densities. Separating them tracks forest turnover even when primary-forest loss and secondary-forest gain leave the combined forest fraction unchanged. Each type has independent area and vegetation-carbon states; V0 and V1 additionally contain age cohorts, and V1 can use distinct leaf traits (Sect. 2.2).

Annual fractions of primary forest (LUH2 primf), secondary forest (secdf) and cropland (the sum of the five LUH2 crop functional types) were taken from the LUH2-GCB2025 reconstruction (Friedlingstein et al., 2026; Hurtt et al., 2020) and aggregated from 0.25° to the 0.5° model grid by 2 × 2 averaging. The same reconstruction provided annual wood-harvest area requests (primf_harv, secmf_harv and secyf_harv), and its management layer supplied the fuelwood fraction of harvested biomass carbon (fulwd; Sect. 2.4). VISIT-2type used cropland fractions from the same reconstruction; in its as-run implementation, the 2019 fraction was held at the 2018 value, whereas the four-type runs used the 2019 update. Nitrogen deposition and fertilizer inputs followed

https://doi.org/10.5194/egusphere-2026-6664
Preprint. Discussion started: 22 November 2026
© Author(s) 2026. CC BY 4.0 License.

the ISIMIP3a histsoc protocol (Frieler et al., 2024). The fraction of other natural vegetation was calculated as the residual of the modelled land area:

$$f_{\text{other}} = 1 - f_{\text{primary}} - f_{\text{secondary}} - f_{\text{cropland}} \quad (1)$$

Negative residual other-vegetation fractions were set to zero. If the four fractions did not sum to one, all four were rescaled to sum to one.

VISIT simulates terrestrial carbon cycling through photosynthesis, autotrophic and heterotrophic respiration, carbon allocation, litterfall and decomposition (Ito, 2010; Ito, 2019). Each grid cell is partitioned into land-cover tiles that share climatic forcing but maintain separate vegetation and soil states. VISIT-4type retains the core process equations for photosynthesis, hydrology and soil carbon turnover. The developments described below concern land-cover states, forest age structure, carbon transfers and wood harvest, together with the secondary-forest trait parameterization described in Sect. 2.2.

The VISIT-2type reference represents land-cover change through net annual changes in cropland area. Cropland expansion clears natural vegetation, whereas abandonment enlarges the natural-vegetation tile while retaining its existing per-area vegetation and soil carbon states. Natural vegetation is represented without age cohorts, and wood harvest is not represented in this reference implementation. VISIT-4type introduces separate primary- and secondary-forest states, area transitions reconstructed from LUH2 annual land-cover fractions and harvest-area requests, six age cohorts per forest type, and wood harvest (Fig. 1; Sects. 2.2–2.4). Sequential configuration comparisons quantify the contributions of these developments, using VISIT-2type as the reference (Sect. 3.2).

https://doi.org/10.5194/egusphere-2026-6664
Preprint. Discussion started: 22 November 2026
© Author(s) 2026. CC BY 4.0 License.

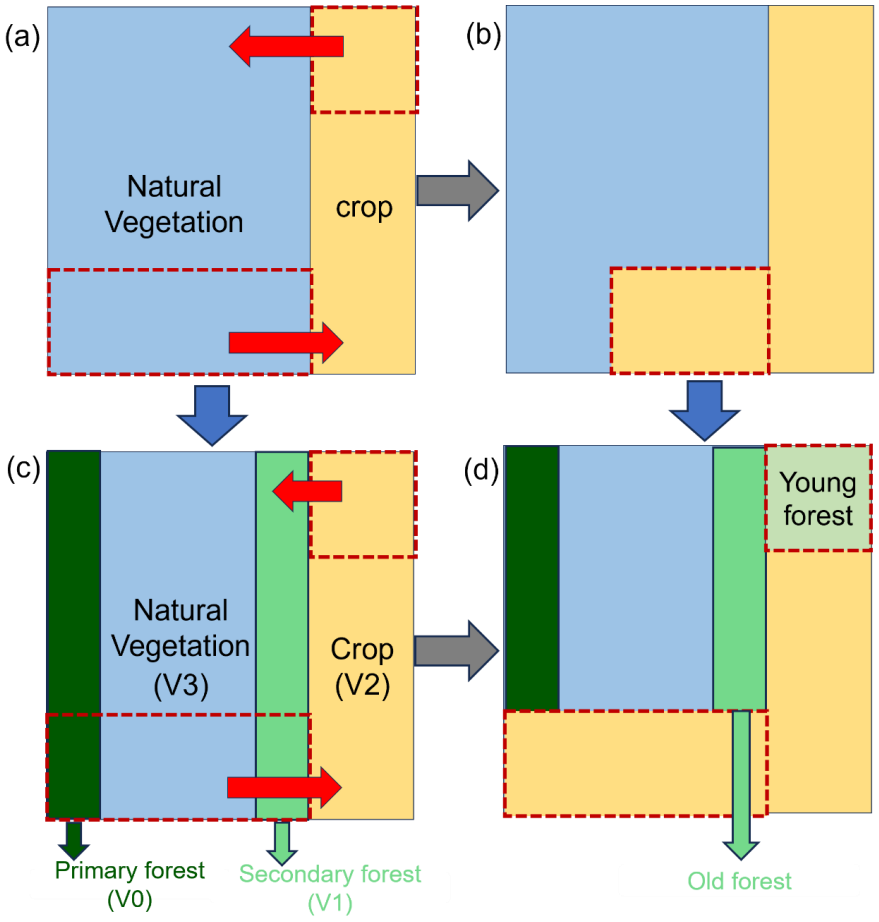


Figure 1. Representation of land-cover change in VISIT. The upper diagrams (a, b) show the two-type scheme with cropland and natural vegetation before and after a year of land-use change; the lower diagrams (c, d) show the same changes in the four-type scheme with primary forest (V0), secondary forest (V1), cropland (V2) and other natural vegetation (V3, including pasture). Red arrows and dashed boxes indicate affected areas. Forest recovery enters V1, allowing its age and carbon density to differ from primary forest.

2.2 Secondary forest parameterization

The four-type configuration retained the original process equations and native Olson-biome parameters, except for a secondary-forest leaf-trait override applied only to V1 (Olson et al., 1983; Ramankutty and Foley, 1999).

We derived V1 specific leaf area (SLA), light-saturated photosynthetic capacity (Pmax), and baseline leaf-turnover rate (lf0) from woody-tree records in TRY (Kattge

https://doi.org/10.5194/egusphere-2026-6664
Preprint. Discussion started: 22 November 2026
© Author(s) 2026. CC BY 4.0 License.

et al., 2020), assigning records to 0.5° Olson-biome grid cells and weighting them by the local LUH2-GCB2025 secondary-forest fraction. For each trait-by-biome combination, we adopted the weighted 75th percentile. Leaf lifespans were first converted to days and inverted to obtain lf0; its upper quartile represents a shorter-lived-leaf strategy corresponding ecologically to a lower-quartile (25th-percentile) lifespan. This growth-oriented choice reflects early-successional resource-acquisitive strategies (Poorter and Bongers, 2006; Poorter et al., 2021) and parallels the upper-quartile SLA used for woody bioenergy crops in ORCHIDEE-MICT-BIOENERGY (Li et al., 2018). Weighted estimates required at least 10 records with non-zero weights (N_w); when N_w was <10 but the raw sample size (N) was at least 10, we used the corresponding unweighted percentile. Otherwise, we retained the native VISIT value.

Because TRY does not identify successional stage, weighting approximates traits in secondary-forest regions rather than exclusively in secondary stands. Olson biome 13 (second-growth woods), lacking a direct TRY counterpart, used tropical evergreen broadleaf-tree observations. V0, V2 and V3 retained native traits. The RC and RD simulations isolated the effect of the V1 override from the other model changes (Sect. 3.2).

https://doi.org/10.5194/egusphere-2026-6664
Preprint. Discussion started: 22 November 2026
© Author(s) 2026. CC BY 4.0 License.

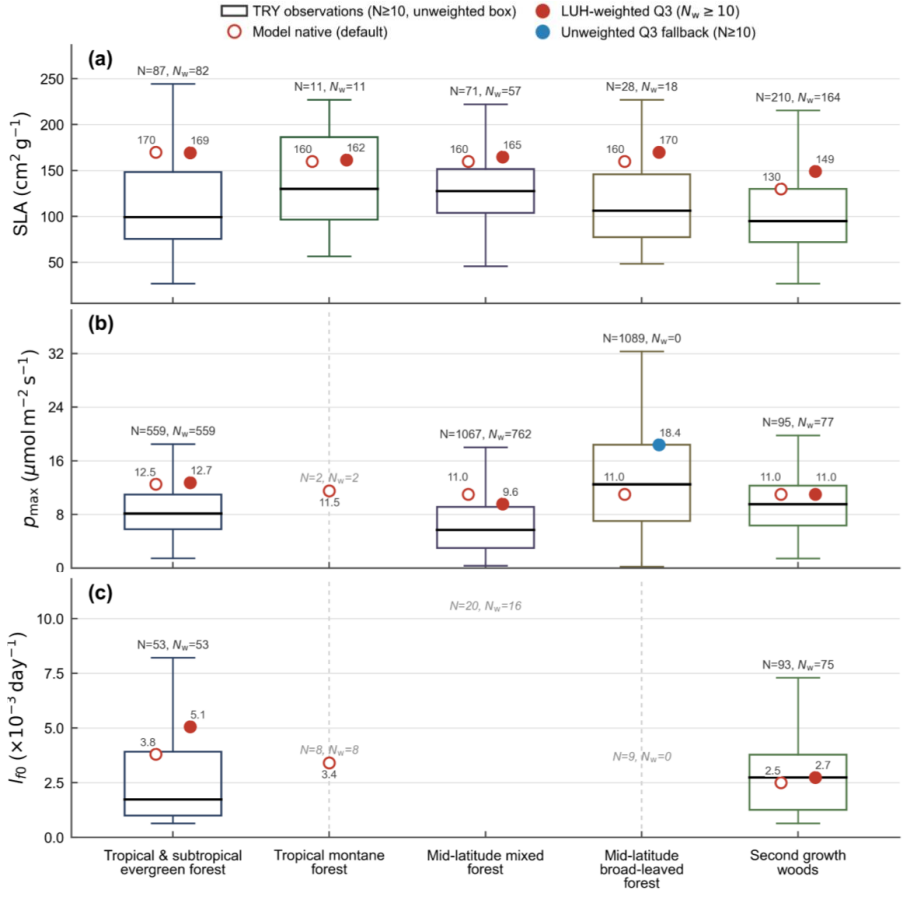


Figure 2. TRY leaf-trait distributions and secondary-forest parameters across Olson forest biomes: (a) specific leaf area (SLA), (b) light-saturated photosynthetic capacity (Pmax) and (c) baseline leaf-turnover rate (lf0). For N ≥ 10, boxes and centre lines denote unweighted interquartile ranges and medians. N is the raw sample size; N_w counts records with non-zero LUH2 secondary-forest weights. Open circles show original VISIT values. Red circles show weighted estimates used when $N_w \geq 10$; blue circles show unweighted estimates used when $N_w < 10$ and N ≥ 10. Updated lf0 and its box are omitted where deciduous phenology controls leaf turnover.

2.3 Forest age cohorts and disturbance

2.3.1 Cohort framework

We introduced sub-grid forest age structure following the cohort concept in the ORCHIDEE forest-management framework (Yue et al., 2018b). Both V0 (primary forest) and V1 (secondary forest) were divided into six age cohorts. Each cohort tracked

https://doi.org/10.5194/egusphere-2026-6664
Preprint. Discussion started: 22 November 2026
© Author(s) 2026. CC BY 4.0 License.

area, mean stand age, leaf-age distribution, phenological state, vegetation-carbon pools, and vegetation-carbon fluxes. V2 (cropland) and V3 (other natural vegetation) remained single land-cover states.

Because forest growth varies among climate zones, we diagnosed grid- and forest-type-specific reference biomass during spin-up. For primary forest (V0) and secondary forest (V1), we recorded vegetation biomass in the third year after establishment as:

$$B_v(t_3) = C_{\mathrm{stem},v}(t_3) + C_{\mathrm{root},v}(t_3) + C_{\mathrm{leaf},v}(t_3) \quad (2)$$

Here, v denotes V0 or V1, and t3 denotes the third year after establishment. Organ-specific reference carbon densities, expressed per unit cohort area, initialized regenerated forest (Sect. 2.3.4). Only live vegetation and its fluxes were age resolved; soil carbon, hydrology and energy exchange remained shared within each land-cover type and received area-weighted cohort fluxes.

2.3.2 Initialization and annual aging

Following spin-up (Sect. 3.1), all primary- and secondary-forest area was initially assigned to Cohort 6 with a nominal stand age of 100 years in 1700. Cohorts 1–5 began with zero area and developed through subsequent harvest, land-use change and regrowth. Thus, the initial forest state was treated as mature rather than drawn from an observed age distribution. Transient land use during 1700–1849 then generated the forest age structure at the start of the historical forcing period.

Stand age was incremented once at the end of each simulation year, after the 12 monthly ecosystem calculations and before end-of-year harvest and the diagnosis of annual land-use fluxes. The start-of-year transition ledger had already updated prescribed land-cover fractions and transferred the associated tile states. Thus, forest established through abandonment or another prescribed gain participated in the monthly calculations of its establishment year and was then incremented at year end. Cohorts were evaluated from oldest to youngest, and a cohort was transferred when its updated mean age reached the upper bound of its age class. This ordering prevents any area from crossing more than one age boundary during a single annual update.

https://doi.org/10.5194/egusphere-2026-6664
Preprint. Discussion started: 22 November 2026
© Author(s) 2026. CC BY 4.0 License.

Cohort 1 represents young stands aged 0–3 years. Forest established through abandonment or other prescribed forest gain was initialized in Cohort 1 at an age of approximately 3 years using the corresponding reference carbon pools. In contrast, harvested area within a forest tile was reinitialized at approximately 1 year using carbon reserved from that year's harvest residue (Sect. 2.3.4). These choices represent sapling establishment and avoid unrealistically slow early growth from very small initial carbon pools. When a cohort advanced to the next class, its area and total vegetation carbon moved together. Where the receiving cohort already contained area, the two states were merged and carbon density and mean age recalculated by area weighting, conserving cohort area and vegetation carbon.

2.3.3 Disturbance priorities and transitions

Start-of-year land-cover changes were recorded in a transition ledger. Harvest and clearing followed an area-first, carbon-follows rule: disturbed area was selected by prescribed cohort priorities, then its leaf, stem and root carbon was transferred. Transfers among the four types were reconstructed from their annual net area changes: after the harvest-linked transfer from primary to secondary forest (A_{log}, below), the remaining losses were allocated to the gaining types in proportion to their gains. This resolves gross forest turnover within a grid cell, including simultaneous primary-forest loss and secondary-forest gain and harvest followed by regrowth within a forest type, whereas opposing transitions between the same pair of types within one year are represented by their net change.

Primary-forest harvest and area change were reconciled to avoid disturbing the same area twice. Let L denote current-year primary-forest net area loss, H the previous year's LUH2 primary-forest harvest request (primf_harv), and G current-year secondary-forest net area gain. We partition L as:

$$\begin{aligned} A_{\mathrm{log}} &= \min(H,\, L,\, G) \\ A_{\mathrm{lc}} &= \min\left(H - A_{\mathrm{log}},\, L - A_{log}\right) \\ A_{\mathrm{dc}} &= L - A_{\mathrm{log}} - A_{\mathrm{lc}} \end{aligned} \tag{3}$$

https://doi.org/10.5194/egusphere-2026-6664
Preprint. Discussion started: 22 November 2026
© Author(s) 2026. CC BY 4.0 License.

Here, A_{log}, A_{lc}, and A_{dc} represent, respectively, the portion of primary-forest loss associated with the previous year's harvest, harvest followed by clearing, and direct clearing. These are bookkeeping allocations that maximize the overlap among the prescribed area changes.

For A_{log}, the post-harvest leaf, stem, and root carbon of the affected area is transferred from primary to secondary forest, with no additional conversion emission. For A_{lc}, clearing is applied to the post-harvest carbon density of the selected cohorts. This allocation represents a plausible land-use sequence in which forest harvest precedes subsequent conversion to agriculture (Asner et al., 2006; Feng et al., 2022). Only A_{dc} is treated as direct clearing of undisturbed primary forest. This area is selected according to the oldest-first rule and therefore carries the carbon density of mature forest. Both A_{log} and A_{lc} are allocated using a youngest-first sequence from Cohort 1 to Cohort 6. If the available area remains insufficient, both segments are reduced proportionally and the unmet area is assigned to direct clearing. Secondary-forest clearing and all other land-cover losses follow the oldest-first rule.

Primary-forest harvest followed the oldest-first rule. Mature secondary-forest harvest selected Cohorts 4 (15 – 30 years), 5 (30 – 50 years) and 6 (⩾50 years); young harvest selected Cohorts 3 (9 – 15 years), 2 (3 – 9 years) and 1 (0 – 3 years) (Table 1). Requests exhausted each cohort before proceeding to the next. Harvested stands reset to Cohort 1 within their forest tile; cleared area moved to cropland or other natural vegetation. Abandonment and other forest gains entered V1 Cohort 1. Removed carbon entered product, residue or emission pathways (Sect. 2.4).

Land-cover fractions and associated tile states were physically transferred once at year start. After monthly ecosystem calculations, annual processing applied biomass burning, aging, harvest and residue routing, then consumed the transition ledger to diagnose conversion emissions, product inputs and root residues without a second physical removal. Product-vintage queues released 10% and 1% of each input over ten and one hundred successive annual positions, respectively, including the input year,

https://doi.org/10.5194/egusphere-2026-6664
Preprint. Discussion started: 22 November 2026
© Author(s) 2026. CC BY 4.0 License.

before NBP diagnosis. Thus, aging and harvest preceded year-end LUC accounting but followed start-of-year area and carbon transfers.

The logging-carry segment transfers standing forest from the primary to the secondary tile. Because each tile's C3/C4 composition is diagnosed from its own surface climate, the receiving secondary tile can have a different C3 fraction in mixed C3/C4 savanna biomes. To conserve transferred carbon, carried cohort carbon density is scaled by the donor-to-recipient C3-fraction ratio when the recipient fraction is larger. When it is smaller, carbon that cannot be retained by the receiving C3 cover enters the secondary tile's litter pool.

2.3.4 Regeneration state

New secondary-forest area arose through two pathways with distinct initial carbon states. Area transferred from primary forest through the logging-carry segment (Alog; Sect. 2.3.3) entered Cohort 1 of V1 and retained the actual post-harvest leaf, stem and root carbon density of the donor stand, subject to the C3-cover adjustment described above. Area created through cropland abandonment or another prescribed forest gain had no donor stand and was initialized from the grid- and forest-type-specific reference state at approximately 3 years. For both abandonment-established forest and harvest-reset forest, target leaf and root carbon densities were multiplied by a sprouting factor of 1.5, whereas target stem carbon was not; target leaf carbon was additionally capped at 60% of local mature primary-forest leaf carbon to avoid excessive initial LAI. Where a valid young-forest reference was unavailable, the model used the local primary-forest reference and then, if necessary, the global median across valid grid cells. Phenological state and leaf-age distribution were reset using hemisphere-specific defaults.

Harvested secondary forest was also reset to Cohort 1 at an age of approximately 1 year. The same leaf- and root-specific sprouting factor and mature-primary-forest leaf-carbon cap defined its target carbon densities, but its realized leaf, stem, and root carbon was limited by the corresponding residue available from that year's harvest. Residue remaining after this reservation entered the litter pathway (Sect. 2.4). Product-

https://doi.org/10.5194/egusphere-2026-6664
Preprint. Discussion started: 22 November 2026
© Author(s) 2026. CC BY 4.0 License.

pool inputs were calculated before the reservation and were therefore unaffected. Because initial sapling carbon was reserved from harvest residue, cells in which nearly all harvested stem wood was fuelwood left little stem residue and regrew from a correspondingly small initial stem pool.

Table 1. Forest age classes and disturbance priorities. Priority 1 denotes the first cohort selected; larger values are used sequentially where higher-priority cohorts contain insufficient area. Priorities apply to harvest and to the direct-clearing segment (A_{dc}) of primary-forest loss. The logging-carry (A_{log}) and harvest-then-clear (A_{lc}) segments follow the young-first sequence from Cohort 1 through Cohort 6; if this sequence cannot supply the requested area, Alog and Alc are reduced proportionally and the balance is assigned to A_{dc} (Sect. 2.3.3).

Cohort	Age interval	Primary harvest	Primary clearing	Mature secondary harvest	Young secondary harvest	Secondary clearing
1	0-3 years	6	6	6	3	6
2	3-9 years	5	5	5	2	5
3	9-15 years	4	4	4	1	4
4	15-30 years	3	3	1	4	3
5	30-50 years	2	2	2	5	2
6	≥50 years	1	1	3	6	1

2.4 Harvested wood products (HWPs), residues, and product-vintage pools

Wood harvest altered forest age structure and redistributed vegetation carbon. Annual harvest-area requests were prescribed from LUH2 and applied to the available forest cohorts following the priorities in Sect. 2.3.3. For cohort i, gross removed stem carbon was calculated as

$$C_{\mathrm{stem},i}^{\mathrm{harv}} = A_i^{\mathrm{harv}} \times S_{\mathrm{stem},i} \quad (4)$$

where A_i^{harv} is harvested cohort area and $S_{\mathrm{stem},i}$ is its simulated pre-harvest stem-carbon density. Grid-cell carbon removals were obtained by multiplying by the forest-tile fraction and by that tile's C3 fraction, which holds the tree carbon. Harvest-area requests were prescribed from LUH2, whereas removed carbon was calculated from

https://doi.org/10.5194/egusphere-2026-6664
Preprint. Discussion started: 22 November 2026
© Author(s) 2026. CC BY 4.0 License.

the simulated cohort state. Leaf and root carbon removed from harvested cohorts were calculated analogously. In RCp, which has no cohorts, harvest removes the requested area fraction of the mean stand.

The LUH2-GCB2025 management layer supplied the fuelwood fraction f of harvested biomass carbon for each grid cell and year (Hurtt et al., 2020). We applied this fraction to gross removed stem carbon, splitting the removal into fuelwood and industrial roundwood pathways following the wood-harvest routines of ORCHIDEE-MICT (Yue et al., 2018b):

$$E_{harv,0} = f\, C_{stem}^{harv} \quad (5a)$$

$$P_{10} = (1 - f)\eta\, c_{10}\, C_{stem}^{harv} \quad (5b)$$

$$P_{100} = (1 - f)\eta\, c_{100}\, C_{stem}^{harv} \quad (5c)$$

$$R_{stem} = (1 - f)[1 - \eta(c_{10} + c_{100})]C_{stem}^{harv} \quad (5d)$$

Here, $E_{harv,0}$ is emitted in the harvest year, P_{10} and P_{100} enter the 10- and 100-year harvested-wood-product pools, and R_{stem} is stem slash. Fuelwood produces no stem slash or product input. Industrial wood is recovered with efficiency $\eta = 0.667$; c_{10} and c_{100} are 0.105 and 0.526 in tropical forests and 0.190 and 0.473 in temperate and boreal forests, respectively. These industrial-harvest coefficients follow ORCHIDEE-MICT; tropical values apply in grid cells whose SAGE potential vegetation is tropical forest and temperate values elsewhere. At $f = 0$, approximately 7.0% and 35.1% of removed stem carbon enter the tropical 10- and 100-year pools; these percentages apply to the industrial portion when fuelwood is present. All affected leaf and root carbon enters the residue pathway before sapling carbon is reserved. The fuelwood fraction was aggregated from 0.25° to 0.5° using LUH2 forest harvest biomass (primf_bioh + secmf_bioh + secyf_bioh) as the weight. The biomass-weighted global fraction was 0.81 in 1850, 0.57 in 1950 and 0.46 in 2019; tropical values were 0.66–0.92.

For LUC clearing, effective biomass comprised cleared leaf and stem carbon plus 80% of cleared root carbon; the remaining 20% of root carbon was assumed to enter litter. Effective biomass was allocated to immediate, 10-year, and 100-year product-vintage pathways using relative weights of 0.40:0.27:0.00 in tropical forests and

https://doi.org/10.5194/egusphere-2026-6664
Preprint. Discussion started: 22 November 2026
© Author(s) 2026. CC BY 4.0 License.

0.40:0.20:0.07 in temperate and boreal forests (McGuire et al., 2001). These weights were normalized by their sum rather than treated as absolute fractions. The weights follow the SAGE potential-vegetation class of the grid cell and apply to all tiles in the cell; non-forest classes use 0.50:0:0 (grassland, tundra, desert and polar desert) or 0.40:0.10:0 (savanna and shrubland). Harvest and clearing used the same product-vintage release module but retained distinct carbon-allocation rules.

The clearing allocation and annual release from product-vintage pools can be written as Eqs. (5e) and (5f), where C_{eff} is effective cleared biomass, w_k is the biome-specific relative allocation weight, E_k is carbon entering pathway k, and I_{10} and I_{100} are annual inputs. Each product vintage releases carbon linearly from its input year: 10% per year for ten years and 1% per year for one hundred years.

$$C_{\text{eff}} = C_{\text{leaf}} + C_{\text{stem}} + 0.8C_{\text{root}},$$
$$E_k = \frac{C_{\text{eff}} w_k}{w_0 + w_{10} + w_{100}}, \qquad k \in \{0,10,100\}. \tag{5e}$$

$$R_{10}(t) = 0.1 \sum_{\tau=t-9}^{t} I_{10}(\tau)$$
$$R_{100}(t) = 0.01 \sum_{\tau=t-99}^{t} I_{100}(\tau) \tag{5f}$$

Before residue was transferred to litter and soil pools, organ-specific carbon was reserved to establish the age-1 cohort in harvested forest. Let C_j^{res} denote available residue of organ j after product allocation and C_j^{sap} the carbon reserved for sapling establishment. Total residue entering soil pools was therefore

$$C_{litter} = \left(C_{stem}^{res} - C_{stem}^{sap}\right) + \left(C_{leaf}^{res} - C_{leaf}^{sap}\right) + \left(C_{root}^{res} - C_{root}^{sap}\right) \tag{6}$$

The remaining residue was partitioned into fast and slow pools:

$$C_{\text{litter}}^{\text{fast}} = x_{\text{ltr}}\left(C_{\text{stem}}^{\text{res}} - C_{\text{stem}}^{\text{sap}}\right) + \alpha_f\left(C_{\text{leaf}}^{\text{res}} - C_{\text{leaf}}^{\text{sap}}\right) + \alpha_r\left(C_{\text{root}}^{\text{res}} - C_{\text{root}}^{\text{sap}}\right) \tag{7a}$$

$$C_{\text{litter}}^{\text{slow}} = (1 - x_{\text{ltr}})\left(C_{\text{stem}}^{\text{res}} - C_{\text{stem}}^{\text{sap}}\right) + \left(1 - \alpha_f\right)\left(C_{\text{leaf}}^{\text{res}} - C_{\text{leaf}}^{\text{sap}}\right) + (1 - \alpha_r)\left(C_{\text{root}}^{\text{res}} - C_{\text{root}}^{\text{sap}}\right) \tag{7b}$$

We used x_{ltr}=0.14 in tropical forests and 0.10 in temperate and boreal forests, with α_f=0.5 and α_r=0.45. Fast and slow residue inputs entered the VISIT litter and

https://doi.org/10.5194/egusphere-2026-6664
Preprint. Discussion started: 22 November 2026
© Author(s) 2026. CC BY 4.0 License.

mineral-soil pools, respectively, and affected heterotrophic respiration (microbial decomposition) from the following simulation year.

2.5 Cohort-level carbon cycling and aggregation

Within V0 and V1, the six cohorts retain independent vegetation-carbon pools, leaf-age distributions, and phenological states. Under shared meteorological forcing and land-cover-level soil and hydrological conditions, canopy photosynthesis, maintenance and growth respiration, carbon allocation, litterfall, and vegetation-carbon change are evaluated for each cohort before area-weighted aggregation (Fig. 3). V2 and V3 retain a single vegetation state.

Full process equations, including the woody-respiration proxy, maintenance and growth respiration, monthly leaf-age update, phenology, disturbance treatment, and cohort aggregation, are provided in Supplementary Methods S1.

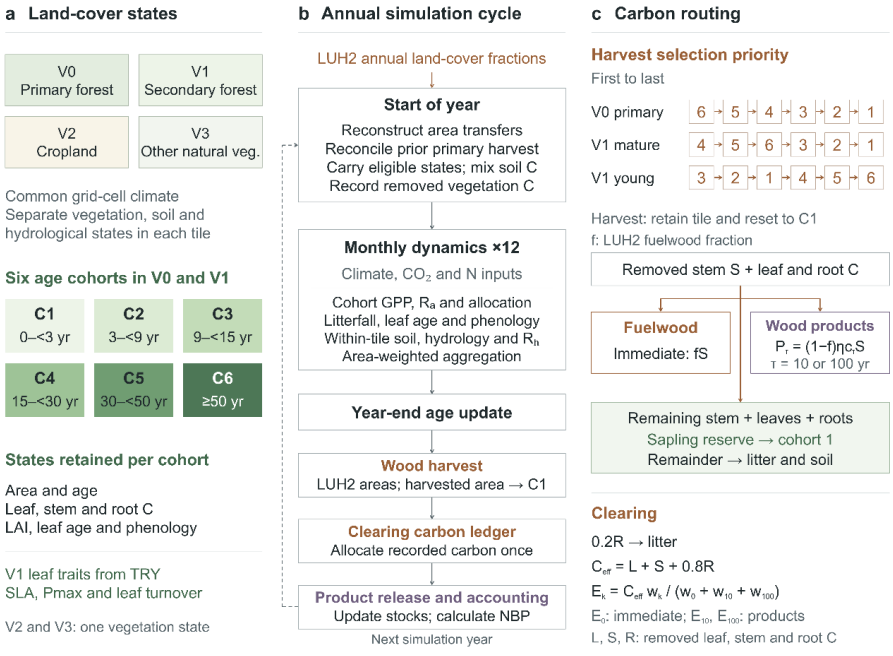


Figure 3. Land-cover states, annual simulation cycle and carbon routing in VISIT-4type. (a) Land-cover tiles, forest age cohorts and the states retained for each cohort. (b) Order of operations within a simulation year; the dashed arrow passes the previous year's primary-forest harvest request to the start-of-year area transfer. Year-end biomass burning, applied before the age update, is not shown. (c) Harvest selection priorities and routing of removed carbon, where f is the LUH2 fuelwood

https://doi.org/10.5194/egusphere-2026-6664
Preprint. Discussion started: 22 November 2026
© Author(s) 2026. CC BY 4.0 License.

fraction, η the industrial-wood recovery efficiency, cτ the product coefficient of the τ-year pool and S the removed stem carbon; for clearing, L, S and R are removed leaf, stem and root carbon and wk the product-pool weights (Sect. 2.4).

3 Simulation design and evaluation

3.1 Spin-up simulations and forest-state initialization

We conducted a long spin-up to equilibrate vegetation, litter, and soil carbon pools. All simulations were global at 0.5° resolution and forced with GSWP3-W5E5 climate data. The 1801-1850 climate sequence was repeated 60 times to provide a 3,000-year spin-up. Daily meteorological variables were aggregated to the monthly model time step. Atmospheric CO_2, land cover, reactive nitrogen deposition, and cropland nitrogen input were fixed at their 1850 values.

V0–V3 were spun up independently to initialize their carbon pools before the transient land-use simulation. Establishment trajectories generated during each simulation's spin-up provided reference leaf, stem and root densities at approximately 3 years for forest gains, approximately 1 year for harvest resets and year 50 for the mature-leaf-carbon cap. Cohort transitions occurred at predefined age boundaries. Convergence was assessed from changes in vegetation carbon, soil carbon and mean NEP between the final two 50-year cycles.

After spin-up, primary- and secondary-forest area was placed in Cohort 6 with nominal age 100 years, and transient land use began in 1700. During 1700–1849, land-cover fractions, harvest areas and fuelwood fractions followed LUH2-GCB2025 annually, while climate repeated the 1801–1850 spin-up sequence, atmospheric CO_2 remained at its pre-industrial spin-up value and nitrogen inputs remained at their 1850 values. This pre-period was excluded from analysis. It allowed the age distribution, product pools and harvest residues at 1850 to develop from the preceding 150 years of land use, moving the mature-forest initialization assumption to 1700. The use of a pre-analysis land-use history is consistent with the rationale of the TRENDY protocol (Sitch

https://doi.org/10.5194/egusphere-2026-6664
Preprint. Discussion started: 22 November 2026
© Author(s) 2026. CC BY 4.0 License.

et al., 2024).

3.2 Historical simulations

We performed six simulations for 1700–2019 with identical climate, atmospheric CO_2, nitrogen deposition and fertilizer forcing and common numerical settings, and analysed 1850–2019 (Table 2). VISIT-2type (R0f) is the reference described in Sect. 2.1. The four-type experiments add processes sequentially: RA uses the four land-cover types and transition ledger without age cohorts or wood harvest, representing each forest tile as one mean stand; RB adds six age cohorts per forest tile; RC adds wood harvest; and RD adds TRY-derived secondary-forest leaf traits. RD is the full VISIT-4type configuration evaluated in Sect. 4.1. RCp adds wood harvest to RA without age cohorts and tests the order of attribution.

Historical environmental forcing followed the ISIMIP3a histsoc configuration (Frieler et al., 2024), with GSWP3-W5E5 meteorology, the historical atmospheric CO_2 series, reactive nitrogen deposition and cropland nitrogen inputs. Annual cropland, primary-forest and secondary-forest fractions, harvest-area requests and fuelwood fractions were supplied by LUH2-GCB2025. Background vegetation distributions were based on the Olson Global Ecosystems and SAGE potential-vegetation datasets.

Each intermediate experiment is a complete model configuration in which a process is represented or absent. With harvest disabled (RA and RB), no harvest carbon is removed, no stand is reset by harvest and no harvest product or residue fluxes are generated. LUH2 primary-harvest area is still passed to the transition ledger, so primary-to-secondary conversion associated with harvest changes the label of the unharvested stand while carrying its carbon state. In RA and RCp, which have no cohorts, forest gains enlarge the mean stand with zero initial biomass. The harvest-then-clear allocation is zero in these experiments, and remaining primary-forest loss is treated as direct clearing. Analyses retained GPP, NPP, NEP, NBP, autotrophic and heterotrophic respiration, and vegetation, litter and soil carbon separately for each land-cover type.

https://doi.org/10.5194/egusphere-2026-6664
Preprint. Discussion started: 22 November 2026
© Author(s) 2026. CC BY 4.0 License.

The total difference, ΔNBP = NBP(RD) − NBP(R0f), was first decomposed into four sequential contrasts: land-cover structure and transitions (RA − R0f), forest age structure (RB − RA), wood harvest (RC − RB) and secondary-forest traits (RD − RC). The first contrast includes separate primary-, secondary- and other-vegetation states, the transition ledger, tile-specific carbon density at clearing and carbon transfer with changing area; it also removes the carbon that VISIT-2type adds to natural vegetation when cropland is abandoned (Sect. 4.3). Age structure adds cohort-specific disturbance and regrowth; harvest adds carbon removals, fuelwood combustion, age resets, product pools, residues and the lower carbon density of harvested-then-cleared stands. The final contrast isolates the TRY-derived SLA, Pmax and leaf turnover of secondary forest.

Each sequential contrast is conditional on processes added before it. Reversing the order of harvest and age structure, using RCp − RA followed by RC − RCp, changed their separate mean NBP contributions by 0.017 Pg C yr^{-1}. The main results therefore use three contrasts that are unaffected by that reversal: land-cover structure and transitions (RA − R0f), wood harvest including forest age structure (RC − RA), and secondary-forest traits (RD − RC). These sum exactly to RD − R0f. The four sequential steps and the alternative order are reported in Tables S1 and S3.

Table 2. Configuration of the six simulations.

Simulation	Land-cover types	Transition ledger	Age cohorts	Wood harvest	Secondary-forest traits
R0f (VISIT-2type)	2	No; net cropland change	No	No	No
RA	4	Yes	No	No	No
RB	4	Yes	Yes	No	No
RC	4	Yes	Yes	Yes	No
RD (VISIT-4type)	4	Yes	Yes	Yes	Yes
RCp	4	Yes	No	Yes	No

https://doi.org/10.5194/egusphere-2026-6664
Preprint. Discussion started: 22 November 2026
© Author(s) 2026. CC BY 4.0 License.

3.3 Evaluation datasets and methods

3.3.1 Site-scale evaluation against eddy-covariance observations

We evaluated forest carbon exchange against eddy-covariance observations from the FLUXNET2015/AmeriFlux data compilation, ICOS, and AsiaFlux-associated JapanFlux and ChinaFlux datasets. The analysis included evergreen needleleaf, evergreen broadleaf, deciduous needleleaf, deciduous broadleaf, and mixed forests. Duplicate site-years were removed and site metadata, units, and flux sign conventions were harmonized (Ueyama et al., 2025; Pastorello et al., 2020).

Annual model fluxes were extracted from the nearest model grid cell to each site and matched by observation year. The evaluated output had no separate forest-type or age-cohort dimension; this comparison therefore assessed grid-cell fluxes at forest-site locations rather than validating individual age cohorts.

The evaluated variables were GPP, ecosystem respiration (R_{eco}), and net ecosystem exchange (NEE). Model R_{eco} was calculated as the sum of autotrophic and heterotrophic respiration. Model NEP was converted to the observational NEE convention as

$$\mathrm{NEE} = -\mathrm{NEP} \tag{8}$$

Positive NEE denotes CO_2 release to the atmosphere. NEE was compared with NEP rather than NBP because eddy-covariance measurements do not include delayed emissions from off-site product pools.

We compared VISIT-2type (R0f) and VISIT-4type (RD) from the simulations in Sect. 3.2. Taylor diagrams summarized the correlation coefficient, standard deviation normalized by the observations and centred RMS difference, calculated across all matched site-years and separately for each site with at least five paired years. For these sites, we report median RMSE, fractions of sites with improved RMSE and correlation, and Wilcoxon signed-rank tests of paired per-site changes. Uncertainty in statistics across all matched site-years was estimated by resampling sites with replacement (2000 bootstrap samples), preserving dependence among years within a site. The same

https://doi.org/10.5194/egusphere-2026-6664
Preprint. Discussion started: 22 November 2026
© Author(s) 2026. CC BY 4.0 License.

statistics were calculated for RA, RB, RC and RCp to attribute changes to model components. Age structure and harvest are reported together, with both sequential orders also assessed.

3.3.2 Grid-scale evaluation against FLUXCOM-X-BASE

We used FLUXCOM-X-BASE as a spatially continuous benchmark for GPP and NEE (Nelson et al., 2024). The product provides monthly 0.5° fluxes for 2001–2021; we evaluated 2001–2019. Monthly fluxes were converted to monthly carbon totals. Model and FLUXCOM data were evaluated on the same grid and common valid-land mask. FLUXCOM NEE was compared with VISIT NEE derived from NEP using Eq. (8).

For each grid cell, RMSE between simulated and FLUXCOM monthly fluxes was calculated over 2001–2019 using months valid in all three datasets. The difference in error between the two configurations was defined as

$$\Delta\mathrm{RMSE}_i = \mathrm{RMSE}_{i,\mathrm{2type}} - \mathrm{RMSE}_{i,\mathrm{4type}} \quad (9)$$

Positive ΔRMSE indicates lower error in VISIT-4type. We report the area-weighted mean ΔRMSE, the fraction of evaluated land area with lower error and zonal means. Uncertainty in area-weighted means was estimated with a spatial block bootstrap (2000 samples), using 5° × 5° blocks for the global mean, 10° × 10° blocks for subsets of cells and 2.5° to 10° blocks as a sensitivity test.

To relate evaluation changes to land use, cells were grouped by their VISIT-4type land-use history over 1851–2019: neither harvest nor forest clearing, harvest only, clearing only, or both. The main classification used a threshold of 1% of cell area for cumulative harvested area and cumulative cleared forest area. Annual cleared area was the primary-forest net loss not assigned to logging carry (Alog), plus secondary-forest net loss (Sect. 2.3.3). Thresholds of 0.1% and 5% and the period 1980–2019 were sensitivity tests. Cells were also grouped by mean secondary-forest fraction over 2001–2019. ΔRMSE was attributed to model components using RA, RB, RC and RCp on the same valid-data mask.

https://doi.org/10.5194/egusphere-2026-6664
Preprint. Discussion started: 22 November 2026
© Author(s) 2026. CC BY 4.0 License.

3.3.3 Forest-state and harvest benchmarking

We compared simulated forest state with the LUH2-GCB2025 states that also supplied the land-use forcing. Secondary-forest vegetation carbon density was compared with LUH2 secmb. Because secmb describes all secondary land, including forest and non-forest, the comparison was restricted to cells in which forest made up at least 80% of LUH2 secondary land and VISIT secondary forest covered at least 1% of the cell. LUH2 carbon density was aggregated to 0.5° using secondary-land area as the weight.

For wood harvest, we compared stem carbon removed from simulated forest stands with LUH2 wood-harvest biomass (primf_bioh + secmf_bioh + secyf_bioh) (Hurtt et al., 2020). Total removed biomass including leaves and roots was reported separately. VISIT was driven by LUH2 harvest-area requests; realized harvest area was compared with those requests, and removed stem carbon per harvested area was used to assess differences in stand carbon density. We also reported carbon routed to immediate fuelwood emissions, 10- and 100-year product pools, litter and soil residues, and the initial biomass of regrowing stands.

3.3.4 Attribution of carbon-flux and stock differences

Global annual fluxes were integrated over all land grid cells. For each contrast in Sect. 3.2, the NBP difference was partitioned into signed contributions from GPP, autotrophic respiration (R_a), heterotrophic respiration (R_h), the reported land-use emission diagnostic (E_{LUC}), and Other:

$$\Delta NBP = \Delta GPP - \Delta R_a - \Delta R_h - \Delta E_{LUC} + \Delta Other \quad (10)$$

E_{LUC} is the model-reported land-use emission: instantaneous conversion emissions, harvest-year fuelwood and releases from the 10- and 100-year product pools, summed over all land-cover types. It includes crop biomass removed when cropland is abandoned, which is not deducted from NBP; Other, defined algebraically as NBP − NEP + E_{LUC}, therefore contains this term, which cancels in ΔNBP. Other otherwise combines fire, crop harvest, dissolved-organic-carbon export, erosion, biogenic volatile

https://doi.org/10.5194/egusphere-2026-6664
Preprint. Discussion started: 22 November 2026
© Author(s) 2026. CC BY 4.0 License.

organic compounds and methane exchange. Harvest residues enter litter and soil and affect R_h.

Flux contributions were averaged over 1850–1939, 1940–1979, 1980–2019 and 1850–2019; full-period means include all 170 output years. Spatial diagnostics were also split among land north of 30° N, between 30° S and 30° N, and south of 30° S. Vegetation, litter and soil stocks were taken from the archived annual output, which averages the 12 monthly stock values. Same-year configuration differences and 2019 annual-mean stocks are reported separately from flux statistics. For Fig. 7c, the difference in each stock between RD and R0f was additionally referenced to its 1850 annual-mean difference. This removes the pre-analysis stock offset from the displayed trajectories. The NBP curve accumulates reported annual RD − R0f differences over 1851–t, giving both curves a zero in 1850. For each configuration, the stock–flux residual over 1851–2019, defined as the change in ecosystem carbon plus product pools minus cumulative NBP, is reported in Table S3e; in VISIT-2type, product pools are part of the litter pool.

4 Results

4.1 Evaluation against eddy-covariance and FLUXCOM X-BASE fluxes

The harmonized pairing table comprised 106 forest sites and 779 site-years, predominantly from Northern Hemisphere mid-latitudes. At sites with at least five paired years, VISIT-4type reduced the RMSE of annual GPP, NEE and ecosystem respiration at 64%, 74% and 74% of sites (56, 42 and 53 sites; Wilcoxon signed-rank test of paired per-site differences, $p = 0.015$, 0.001 and 0.001), and the median RMSE decreased from 615 to 565, 303 to 286 and 499 to 434 g C m^{-2} yr^{-1}, respectively. In contrast, the correlation with the observations improved at only 43%, 62% and 42% of the sites, and none of these changes was significant ($p \geq 0.198$). The Taylor diagrams of all paired site-years show the same pattern (Figs. 4 and S1): the two configurations

https://doi.org/10.5194/egusphere-2026-6664
Preprint. Discussion started: 22 November 2026
© Author(s) 2026. CC BY 4.0 License.

have similar correlations (0.465 and 0.481 for GPP, −0.074 and 0.046 for NEE), and VISIT-4type has a slightly smaller centred RMS difference (759 and 734 g C m^{-2} yr^{-1} for GPP, 376 and 368 g C m^{-2} yr^{-1} for NEE). The four-type framework thus reduced error magnitude rather than improving interannual variability, and NEE correlations remained low.

The lower errors came with lower simulated fluxes. Mean simulated GPP at the sites was 44 g C m^{-2} yr^{-1} lower in VISIT-4type and ecosystem respiration 54 g C m^{-2} yr^{-1} lower, mainly through wood harvest including age structure (−27 and −31 g C m^{-2} yr^{-1}) and the secondary-forest traits (−13 and −9 g C m^{-2} yr^{-1}; Table S1). The positive bias of ecosystem respiration was almost halved (121 to 67 g C m^{-2} yr^{-1}) and that of NEE decreased (221 to 212 g C m^{-2} yr^{-1}), whereas the negative GPP bias increased (−104 to −148 g C m^{-2} yr^{-1}).

https://doi.org/10.5194/egusphere-2026-6664
Preprint. Discussion started: 22 November 2026
© Author(s) 2026. CC BY 4.0 License.

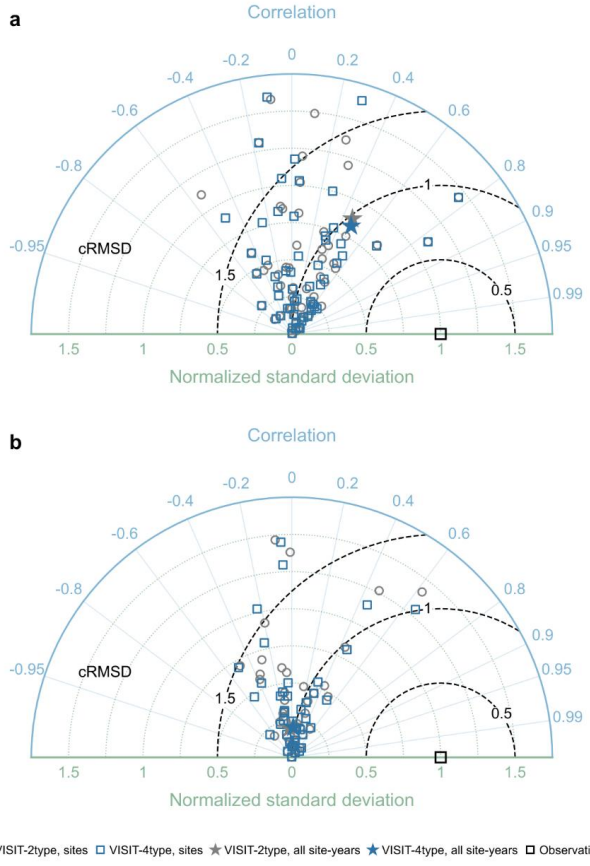


Figure 4. Taylor diagrams of annual (a) GPP and (b) NEE simulated by VISIT-2type and VISIT-4type against eddy-covariance observations. Grey open circles and blue open squares show sites with at least five paired years (56 sites for GPP, 42 for NEE); filled grey and blue stars show all paired site-years (696 and 503), respectively. The blue outer arc gives correlation, the green radial scale gives standard deviation normalized by the observations, and black dashed arcs give normalized centred RMS difference (cRMSD) of 0.5, 1.0 and 1.5 from the observational reference (black open square). NEE = −NEP; positive values denote release to the atmosphere.

Against monthly FLUXCOM X-BASE fluxes over 2001–2019, the area-weighted RMSE decreased from 54.23 to 53.81 g C m^{-2} $month^{-1}$ for GPP (58 487 grid cells, 131.7 × 10^6 km^2) and from 22.41 to 22.16 g C m^{-2} $month^{-1}$ for NEE (58 513 cells). The mean ΔRMSE of +0.42 g C m^{-2} $month^{-1}$ for GPP and +0.25 g C m^{-2} $month^{-1}$ for NEE was robust to spatial autocorrelation (95% intervals 0.25–0.59 and 0.19–0.31 from a bootstrap of 5° × 5° blocks, and positive for blocks of 2.5° to 10°). The error decreased

https://doi.org/10.5194/egusphere-2026-6664
Preprint. Discussion started: 22 November 2026
© Author(s) 2026. CC BY 4.0 License.

over 46.7% of the evaluated area for GPP and 56.1% for NEE, with the largest band-mean improvement between 30° S and 30° N (Fig. 5a, b, d, e).

The mean improvement was concentrated in grid cells with a history of wood harvest or forest clearing (Fig. 5c, f). In cells where neither the cumulative harvested area nor the cumulative cleared forest area exceeded 1% of the cell over 1851–2019 (67% of the evaluated area), ΔRMSE was indistinguishable from zero (GPP −0.03, 95% interval −0.07 to 0.01; NEE 0.00, −0.01 to 0.02 g C m^{-2} $month^{-1}$). ΔRMSE was positive in cells with clearing only (GPP +1.54, NEE +0.43 g C m^{-2} $month^{-1}$; 4% of the area) and in cells with both harvest and clearing (+1.46 and +0.88; 25% of the area), which together accounted for almost the entire global mean improvement. In cells with harvest only (4% of the area), NEE improved (+0.37) and GPP changed by an amount within its uncertainty (+0.44, −0.32 to 1.16). Grouped by the 2001–2019 mean secondary-forest fraction, ΔRMSE was near zero where secondary forest covered less than 0.1% of the cell and largest where it covered 10–20% (Fig. S2a, b).

Within each group, the improvement came from the process that acts there (Fig. S2c, d). In cells with clearing only, the land-cover structure and transitions contributed 1.37 of the 1.54 g C m^{-2} $month^{-1}$ GPP improvement and all of the NEE improvement; in cells with harvest only, wood harvest including age structure contributed the improvement (GPP +0.81, NEE +0.46). The secondary-forest traits increased the error in harvested cells (GPP −0.38 in cells with harvest only, NEE −0.27 in cells with both) but decreased it in cells with clearing only (GPP +0.19). Globally, the land-cover structure and transitions contributed +0.08 (GPP) and +0.19 g C m^{-2} $month^{-1}$ (NEE), wood harvest including age structure +0.38 and +0.14, and the traits −0.04 and −0.07 (Table S1).

https://doi.org/10.5194/egusphere-2026-6664
Preprint. Discussion started: 22 November 2026
© Author(s) 2026. CC BY 4.0 License.

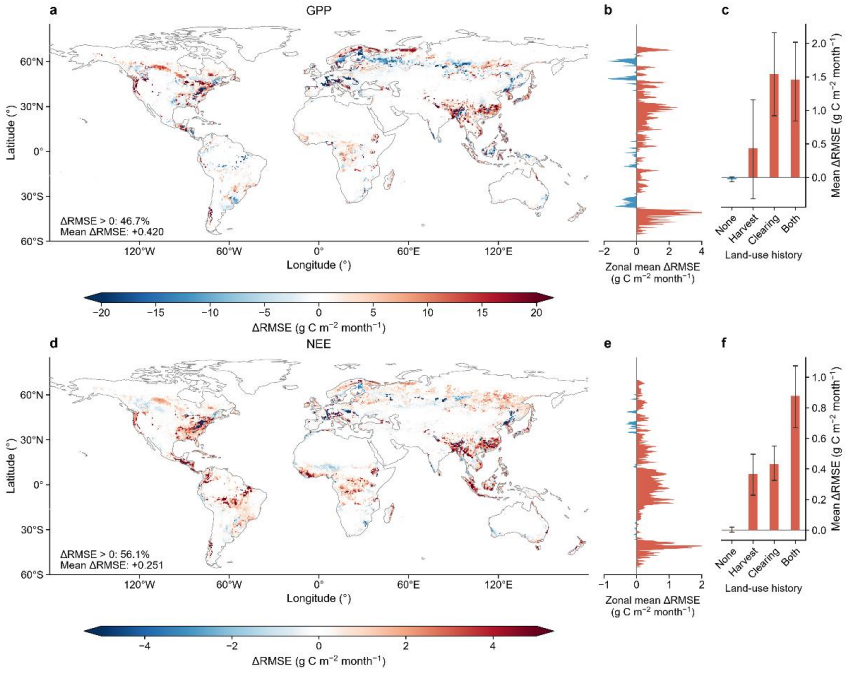


Figure 5. Change in the RMSE of monthly (a) GPP and (d) NEE against FLUXCOM X-BASE over 2001–2019, ΔRMSE = RMSE(VISIT-2type) − RMSE(VISIT-4type); positive values (red) indicate lower error in VISIT-4type. (b, e) Area-weighted zonal means. (c, f) Area-weighted mean ΔRMSE of grid cells grouped by their land-use history in VISIT-4type over 1851–2019: no harvest or clearing (None), wood harvest only (Harvest), forest clearing only (Clearing) and both (Both); a cell counts as harvested or cleared when the cumulative area exceeds 1% of the cell. Error bars are 95% intervals from a bootstrap of 10° × 10° blocks. Cells with identical RMSE in both configurations and cells with fewer than 12 valid months are left blank in (a, d).

4.2 Harvested carbon in VISIT-4type and LUH2

LUH2-GCB2025 prescribes the areas of land-cover change and wood harvest; its wood-harvest biomass (*_bioh) and secondary-land biomass (secmb) are diagnosed by its land-use model rather than observed. Realized harvest area in VISIT-4type was approximately 98% of the request, so differences in harvested carbon mainly reflect the carbon density of the harvested stands. Stem carbon of the harvested stands, the VISIT quantity comparable to LUH2 wood-harvest biomass, increased from 0.18 Pg C yr^{-1} in 1850–1939 to 0.47 in 1940–1979 and 0.70 Pg C yr^{-1} in 1980–2019, compared with 0.40,

https://doi.org/10.5194/egusphere-2026-6664
Preprint. Discussion started: 22 November 2026
© Author(s) 2026. CC BY 4.0 License.

0.85 and 1.14 Pg C yr^{-1} in LUH2 (Fig. 6a; Table S2). The two series followed the same trajectory, and their ratio increased from 0.44 to 0.61. Including leaves and roots, VISIT-4type removed 0.24, 0.60 and 0.91 Pg C yr^{-1}.

Per harvested area, VISIT-4type removed 38 Mg C ha^{-1} of stem carbon from primary forest in 1850–1939 and 69 Mg C ha^{-1} in 1980–2019, compared with 73 and 93 Mg C ha^{-1} implied by LUH2 (Fig. 6b). Because harvest removes all vegetation from the selected area, total removal per harvested hectare equals the vegetation carbon of the harvested stands, 48 and 84 Mg C ha^{-1} in primary forest in the two periods. Secondary-forest harvest accounted for 58% of the 1980–2019 stem-carbon gap. Ninety per cent of the secondary harvest area came from LUH2 young-forest requests, for which LUH2 implies 5.1 Mg C ha^{-1} and VISIT-4type removed 1.8 Mg C ha^{-1} of stem carbon; for mature secondary forest, the corresponding values were 73 and 32 Mg C ha^{-1}. In the harvested cells, VISIT secondary forest held 15 Mg C ha^{-1} of vegetation carbon in the year before harvest. The gap therefore reflects the lower simulated carbon density of harvested primary forest and of the young secondary forests that dominate the harvest requests. Across cells where forest dominates LUH2 secondary land, VISIT secondary-forest vegetation carbon was 46, 42 and 43 Mg C ha^{-1} in the three periods, 21%, 16% and 12% below LUH2 secmb (Fig. 6c).

https://doi.org/10.5194/egusphere-2026-6664
Preprint. Discussion started: 22 November 2026
© Author(s) 2026. CC BY 4.0 License.

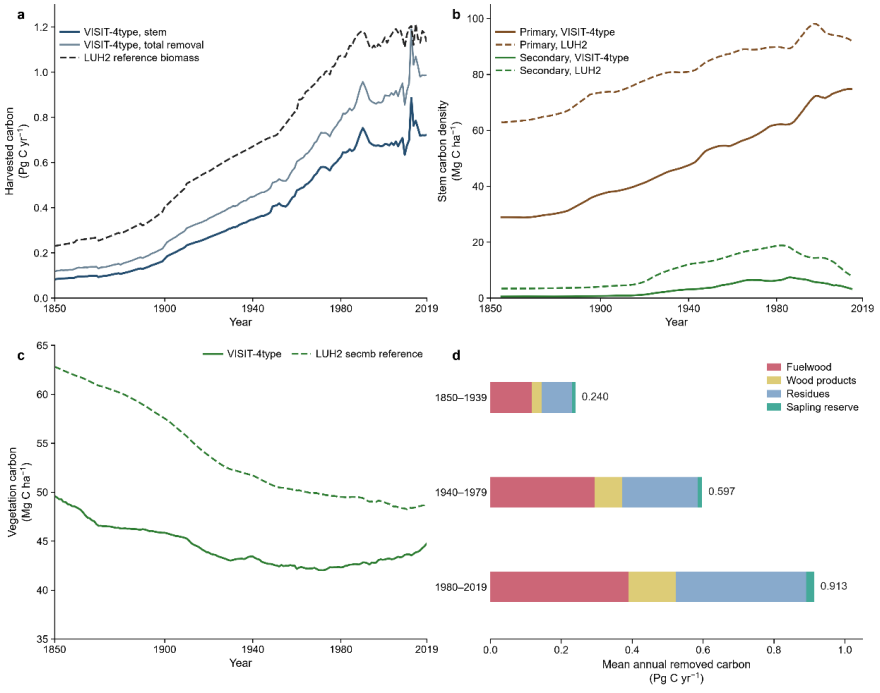


Figure 6. Wood harvest in VISIT-4type compared with the LUH2-GCB2025 forcing. (a) Annual global harvested stem carbon, total removal including leaves and roots, and LUH2 wood-harvest biomass. (b) Stem carbon removed per harvested area in primary and secondary forest, calculated as the ratio of carbon and area sums in complete 11-year centred windows (1855–2014). (c) Annual secondary-forest vegetation carbon density in VISIT-4type and LUH2 secondary mean biomass (secmb), restricted to cells where forest makes up at least 80% of LUH2 secondary land and VISIT secondary forest covers at least 1% of the cell. Solid lines represent VISIT-4type and dashed lines LUH2. (d) Period-mean annual removal partitioned into fuelwood, product-pool inputs, residues and sapling reservation; numbers at bar ends give total removal in Pg C yr^{-1}. VISIT-4type is driven by LUH2 harvest-area requests; realized area is approximately 98% of the request (Table S2).

4.3 Attribution of differences in carbon fluxes and stocks

Annual global NBP of the two configurations was highly correlated (r = 0.997), but VISIT-4type was lower in 169 of the 170 years (Fig. 7b). Mean NBP was 0.704 Pg C yr^{-1} in VISIT-2type and 0.531 Pg C yr^{-1} in VISIT-4type over 1850–2019, and 1.670 and 1.478 Pg C yr^{-1} over 1980–2019. The mean configuration differences were therefore −0.173 and −0.192 Pg C yr^{-1} for the full and recent periods, respectively. Absolute NBP of all six configurations is shown in Fig. S3c.

https://doi.org/10.5194/egusphere-2026-6664
Preprint. Discussion started: 22 November 2026
© Author(s) 2026. CC BY 4.0 License.

Wood harvest including age structure contributed −0.171 Pg C yr⁻¹ to the full-period NBP difference, while land-cover structure and transitions contributed +0.026 and secondary-forest traits −0.027 Pg C yr⁻¹ (Fig. 7b; Table S3b). The age and harvest terms are combined because their separate contributions depend on their order: age structure added before harvest changed NBP by only −0.009 Pg C yr⁻¹, and reversing their order changed the separate contributions by 0.017 Pg C yr⁻¹. Without harvest, 13% of secondary-forest area was younger than 50 years in 2019, compared with 42% with harvest. The combined harvest contribution increased in magnitude from −0.083 Pg C yr⁻¹ in 1850–1939 to −0.210 in 1940–1979 and −0.333 in 1980–2019; the trait contribution changed from −0.010 to −0.075 Pg C yr⁻¹. Land-cover structure and transitions changed sign, contributing −0.065, +0.040 and +0.217 Pg C yr⁻¹ across the three periods.

The negative contribution was concentrated where forests were harvested or cleared (Fig. S3d; Table S3). Grid cells in which both cumulative harvest and forest clearing exceeded 1% of the cell over 1851–2019, 25% of the land area, contributed −0.228 Pg C yr⁻¹, whereas cells without forest harvest or clearing (67% of the land) contributed +0.085 Pg C yr⁻¹, almost entirely through the land-cover structure and transitions. Between 30° S and 30° N the difference was −0.105 Pg C yr⁻¹ and north of 30° N −0.070 Pg C yr⁻¹, with harvest dominating in both bands (−0.106 and −0.060 Pg C yr⁻¹).

The flux contributions show a strong compensation between production and respiration (Fig. 7a, d). Over 1850–2019, GPP was 1.426 Pg C yr⁻¹ lower in VISIT-4type, while lower Ra and Rh contributed +0.806 and +0.873 Pg C yr⁻¹ to the sink, respectively. Their sum gave a NEP difference of +0.253 Pg C yr⁻¹. Higher reported land-use emissions contributed −0.494 Pg C yr⁻¹ and Other +0.068 Pg C yr⁻¹, yielding the NBP difference of −0.173 Pg C yr⁻¹. The recent-period budget in Fig. 7a shows the same compensation at larger magnitude: $\Delta GPP = -2.461$, $-\Delta Ra = +1.421$, $-\Delta Rh = +1.559$, $-\Delta E_{LUC} = -0.848$ and $\Delta Other = +0.137$ Pg C yr⁻¹, summing to −0.192 Pg C

https://doi.org/10.5194/egusphere-2026-6664
Preprint. Discussion started: 22 November 2026
© Author(s) 2026. CC BY 4.0 License.

yr⁻¹. Thus lower GPP alone does not explain the lower NBP.

The three contrasts affect different parts of this budget (Fig. S4). Wood harvest including age structure lowered GPP by 0.596 Pg C yr⁻¹, while lower Ra and Rh contributed +0.291 and +0.331 Pg C yr⁻¹, giving a small net NEP effect of +0.026 Pg C yr⁻¹. Its reported land-use emission contribution was −0.216 Pg C yr⁻¹. Secondary-forest traits lowered GPP by 0.496 Pg C yr⁻¹, with compensating respiration contributions of +0.277 and +0.168 Pg C yr⁻¹ and a NEP effect of −0.052 Pg C yr⁻¹. In the gridded GPP diagnostic, 86% of this reduction occurred in tropical and subtropical evergreen forest (Olson type 1), where the TRY-derived leaf turnover rate is one third higher than the native value while SLA and Pmax are nearly unchanged. The mean GPP change followed the LAI change (r = 0.97 across 17 186 cells with a mean secondary-forest fraction of at least 1%). Land-cover structure and transitions contributed GPP −0.334, −ΔRa +0.238 and −ΔRh +0.375 Pg C yr⁻¹, giving ΔNEP +0.279 Pg C yr⁻¹, alongside $-\Delta E_{LUC}$ = −0.292 Pg C yr⁻¹. Its small net NBP contribution therefore combines larger opposing terms.

The configurations also differed in annual-mean carbon stocks (Fig. 7c; Table S3a, b). In 2019, vegetation carbon was 68.5 Pg C lower in VISIT-4type than in VISIT-2type and litter plus soil carbon was 25.4 Pg C lower, giving a same-year ecosystem-stock difference of −93.9 Pg C. The corresponding ecosystem-stock difference in 1850 was already −12.7 Pg C following the pre-analysis land-use history. Relative to that 1850 annual-mean contrast, the change in the ecosystem-stock difference reached −81.2 Pg C in 2019: −58.7 Pg C in vegetation and −22.5 Pg C in litter plus soil.

The cumulative reported NBP difference over 1851–2019 was −29.2 Pg C, 52.0 Pg C less negative than the baseline-referenced ecosystem-stock difference of −81.2 Pg C (Fig. 7c). Most of this gap arises because abandoned cropland in VISIT-2type joins natural vegetation at the existing per-area vegetation and soil carbon of that tile, so that stocks increase without an uptake flux. Over 1851–2019, ecosystem stocks in VISIT-2type increased by 56.6 Pg C more than its cumulative NBP, whereas the corresponding

https://doi.org/10.5194/egusphere-2026-6664
Preprint. Discussion started: 22 November 2026
© Author(s) 2026. CC BY 4.0 License.

residual in VISIT-4type, where new forest starts from sapling carbon and soil carbon is mixed by area, was 11.7 Pg C including product pools (Table S3e). Of the 52.0 Pg C gap, 46.8 Pg C occurred in grid cells where cumulative cropland abandonment exceeded 1% of the cell area.

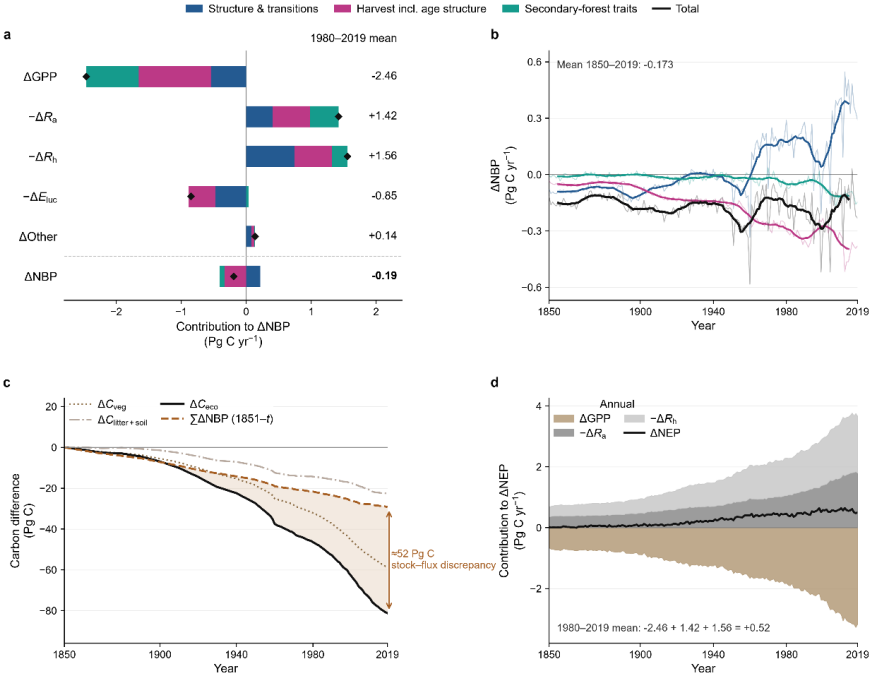


Figure 7. Attribution of global carbon-flux and stock differences between VISIT-4type and VISIT-2type (RD − R0f), split into land-cover structure and transitions (RA − R0f), wood harvest including age structure (RC − RA) and secondary-forest traits (RD − RC). Positive flux contributions increase the land sink; E_{LUC} is the model-reported land-use emission and Other = NBP − NEP + E_{LUC} (Sect. 3.3.4). (a) Contributions of ΔGPP, −ΔRa, −ΔRh, −ΔE_{LUC} and ΔOther to the 1980–2019 mean ΔNBP (Pg C yr^{-1}); diamonds mark totals. (b) Annual ΔNBP by contrast (thin lines) and 11-year centred means (thick lines, 1855–2014). (c) Annual-mean vegetation, litter-plus-soil and ecosystem carbon differences relative to 1850, compared with cumulative ΔNBP since 1851. The shaded gap (52.0 Pg C in 2019) arises from carbon added to natural vegetation on abandoned cropland in VISIT-2type (Sect. 4.3). (d) Annual ΔGPP, −ΔRa and −ΔRh, with their sum ΔNEP (black line). Full component time series are shown in Fig. S4.

https://doi.org/10.5194/egusphere-2026-6664
Preprint. Discussion started: 22 November 2026
© Author(s) 2026. CC BY 4.0 License.

5 Discussion

5.1 Forest states and carbon transfers under land-use change

Forest state, not only forest extent, determines the carbon consequences of land use in VISIT-4type. Grid cells with the same combined forest fraction can hold old carbon-rich stands, recently harvested stands or recovering secondary forest, with different stocks and flux trajectories. In 1980–2019, harvest removed 0.91 Pg C yr^{-1} of vegetation carbon, of which 43% was assigned to fuelwood, 40% to residues and 15% to product inputs; fuelwood combustion, residue decomposition and product release operate on different timescales (Mason Earles et al., 2012; Peng et al., 2023). Lower GPP in the harvested landscape was largely compensated by lower autotrophic and heterotrophic respiration (Fig. S4a–c), so the combined harvest contrast changed NEP much less than NBP, and the NBP response was set by the amount of carbon removed and its routing.

Age structure links each disturbance to the carbon density and recovery stage of the affected forest. With harvest, 42% of secondary forest was younger than 50 years in 2019, compared with 13% without harvest. Adding cohorts without harvest changed NBP by only −0.009 Pg C yr^{-1}, and the 0.017 Pg C yr^{-1} order dependence shows that age structure matters mainly where disturbance repeatedly creates young stands. Disturbance removes carbon accumulated in older stands (Besnard et al., 2025), and regrowth restores it only gradually (Pugh et al., 2019; Yue et al., 2018a). The magnitude of this effect depends on the regeneration states and disturbance priorities used in VISIT.

How carbon moves with area matters as much as which transitions are represented. Changing a tile's area while retaining its per-area state changes the grid-cell stock without any flux. When cropland is abandoned, VISIT-2type enlarges natural vegetation at its existing per-area vegetation and soil carbon, which produces the 52 Pg C stock–flux gap in Fig. 7c. VISIT-4type transfers soil carbon by area, carries post-harvest forest states and starts new forest from sapling carbon, which reduces the stock–

https://doi.org/10.5194/egusphere-2026-6664
Preprint. Discussion started: 22 November 2026
© Author(s) 2026. CC BY 4.0 License.

flux residual from 56.6 Pg C in VISIT-2type to 11.7 Pg C (Table S3e). In grid cells without forest harvest or clearing, the land-cover structure contrast increased NBP by 0.085 Pg C yr^{-1}, mainly through lower heterotrophic respiration, consistent with the decomposition of carbon inherited on abandoned cropland in VISIT-2type.

5.2 Implications for model evaluation and land-use applications

Fluxes and stocks provide complementary constraints. Eddy-covariance and FLUXCOM comparisons constrain ecosystem fluxes but not NBP, off-site product releases or age-specific biomass, and FLUXCOM shares information with the eddy-covariance networks. Biomass maps, forest inventories, soil-carbon observations and stand-age-resolved measurements are needed to test the stock differences in Fig. 7c. This matters for projections because forest carbon density sets both the initial state of regrowth and the carbon exposed to future clearing or harvest.

Net-versus-gross land-use studies show that simultaneous gains and losses and the treatment of disturbed biomass alter simulated land-use effects (Hansis et al., 2015; Wilkenskjeld et al., 2014). VISIT-4type resolves gross forest turnover reconstructed from annual LUH2 states and harvest requests; using the complete LUH2 transition matrix would add opposing transitions between the same land-cover types. The −0.173 Pg C yr^{-1} NBP difference is a configuration contrast within VISIT rather than an independent estimate of historical E_{LUC}.

Secondary-forest traits changed GPP by −0.496 Pg C yr^{-1} but NBP by only −0.027 Pg C yr^{-1}, because lower autotrophic and heterotrophic respiration offset most of the GPP change. The traits reduced GPP error in cells with clearing only but increased errors in harvested cells, and did not consistently improve global or site statistics (Fig. S2; Table S1). TRY records lack successional-stage and stand-age labels, so weighting by secondary-forest area approximates the traits of secondary-forest regions rather than of regrowing stands. Trait, flux and biomass measurements from regrowing stands are needed to constrain these parameters (Chazdon et al., 2016; Kattge et al., 2020; Poorter et al., 2021).

https://doi.org/10.5194/egusphere-2026-6664
Preprint. Discussion started: 22 November 2026
© Author(s) 2026. CC BY 4.0 License.

The largest NBP difference occurred between 30° S and 30° N (−0.105 Pg C yr^{-1}), where losses of carbon-dense forest, secondary-forest formation, agricultural expansion and harvest occur together. Tropical land use is more diverse than the transitions represented here (Bourgoin et al., 2024; Bousfield and Edwards, 2025). Managed plantations and lignocellulosic bioenergy systems differ in rotation length, allocation, harvest frequency, residue management and product fate, and their absence may contribute to the lack of improvement in parts of tropical South America and Southeast Asia (Fig. 5). Representing them as managed land-cover types is a priority for applications to land-based mitigation (Li et al., 2018).

6 Conclusions

We developed VISIT-4type, which separates primary and secondary forest, resolves six forest age cohorts, transfers carbon with changing area through a transition ledger and represents wood harvest with fuelwood and industrial-wood pathways. The framework reduced per-site annual GPP, NEE and ecosystem-respiration errors against eddy-covariance observations, and grid-scale error reductions against FLUXCOM X-BASE were concentrated in landscapes with harvest or clearing.

Over 1850–2019, global NBP was 0.173 Pg C yr^{-1} lower than in the two-type reference, almost entirely through wood harvest with forest age structure (−0.171 Pg C yr^{-1}). Lower GPP was largely offset by lower autotrophic and heterotrophic respiration, so the NBP difference was set mainly by land-use carbon losses. The carbon density of disturbed stands and the routing of removed biomass therefore control the simulated land-use effect. Annual-mean ecosystem stocks were 93.9 Pg C lower in VISIT-4type in 2019. Relative to 1850, the stock difference exceeded the cumulative NBP difference by 52 Pg C, mainly because abandoned cropland in VISIT-2type inherits natural-vegetation carbon without an uptake flux (the remaining 7.0 Pg C is held in VISIT-4type product pools); the transition ledger and sapling-based regrowth reduce the stock–flux residual from 56.6 Pg C in VISIT-2type to 11.7 Pg C in VISIT-4type. Forest

https://doi.org/10.5194/egusphere-2026-6664
Preprint. Discussion started: 22 November 2026
© Author(s) 2026. CC BY 4.0 License.

inventories and biomass maps are needed to test the simulated stocks.

The TRY-derived secondary-forest traits did not consistently improve evaluation, and their NBP effect was small because respiration offset most of the GPP change. Observations that resolve stand age and successional stage, better-constrained pre-1850 land-use histories and explicit managed plantations will strengthen future applications. Further development will add crop-specific traits and management for eucalypt plantations in tropical and subtropical regions and for poplar, willow and switchgrass in other suitable climates.

Code and data availability

The VISIT-4type v1.0 source code, the VISIT-2type reference configuration, the build configurations of all six simulations and the input-preprocessing and output-conversion tools are archived on Zenodo under the GNU General Public License v3.0 or later (GPL-3.0-or-later) (Dong, 2026; https://doi.org/10.5281/zenodo.24367012). The same archive contains all model inputs (including the ISIMIP3a forcing), the evaluation data, the model output and the scripts used to produce all figures and tables, as described below.

Land-use forcing (land-cover fractions, wood-harvest areas, fuelwood fractions and the 1700–1849 land-use history) was derived from the LUH2-GCB2025 reconstruction (Friedlingstein et al., 2026; Hurtt et al., 2020). Because this release is distributed through a project website (https://luh.umd.edu/data.shtml) rather than a long-term archive, the LUH2-GCB2025 variables used in this study are re-published in the Zenodo archive at their original 0.25° resolution for 1700–2019, under their original CC BY-SA 4.0 licence, together with the 0.5° model input files derived from them and the static maps read by VISIT. Climate forcing (GSWP3-W5E5), nitrogen deposition and nitrogen fertilizer inputs follow the ISIMIP3a protocol (Frieler et al., 2024) and were taken from the ISIMIP Repository (Lange et al., 2022; Volkholz and Ostberg, 2020; Yang and Tian, 2020). To ensure their long-term availability, these data are also re-

https://doi.org/10.5194/egusphere-2026-6664
Preprint. Discussion started: 22 November 2026
© Author(s) 2026. CC BY 4.0 License.

published in the Zenodo archive under their original CC0 1.0 licence: the nitrogen-deposition and nitrogen-fertilizer data as the original ISIMIP3a files, and the climate data as the monthly means of daily near-surface air temperature, precipitation, near-surface specific humidity and surface downwelling shortwave radiation for 1801–2019, which are the values read by VISIT on its monthly time step. The archived code includes the program that computes these monthly means from the daily ISIMIP3a data and writes all ISIMIP3a-based model input files, and the archived model input includes the annual atmospheric CO_2 concentrations read by VISIT.

The evaluation data are re-published in the Zenodo archive in the form used in this study: the harmonized annual eddy-covariance data of the 106 forest sites, compiled from the FLUXNET2015/AmeriFlux data compilation (Pastorello et al., 2020; https://fluxnet.org/data/fluxnet2015-dataset/), the Integrated Carbon Observation System (ICOS) Ecosystem Thematic Centre Level 2 INTERIM release 2025-2 (https://doi.org/10.18160/R3G6-Z8ZH), JapanFlux2024 (Ueyama et al., 2025; https://db.cger.nies.go.jp/asiafluxdb/); and ChinaFlux; the FLUXCOM X-BASE monthly GPP and NEE for 2001–2019 (Nelson et al., 2024; https://doi.org/10.18160/5NZG-JMJE); the LUH2-GCB2025 benchmark fields aggregated to 0.5°; and the secondary-forest leaf traits derived from the TRY Plant Trait Database (Kattge et al., 2020; https://www.try-db.org; data request no. 48805). Re-published third-party data retain their original licences (CC BY 4.0, or CC BY-SA 4.0 for LUH2-GCB2025), and the original sources should be cited when they are reused. Individual TRY records are not redistributed and can be requested from https://www.try-db.org.

The archive also contains the annual gridded output of the six simulations for 1850–2019, the land-use and harvest diagnostics of the four-type simulations, global annual time series, and the scripts and intermediate data used to produce all figures and tables.

https://doi.org/10.5194/egusphere-2026-6664
Preprint. Discussion started: 22 November 2026
© Author(s) 2026. CC BY 4.0 License.

Author contributions

JD: conceptualization, methodology, software (model development), investigation (simulations), formal analysis, data curation, visualization and writing – original draft. SZ: data curation (eddy-covariance and plant-trait data), validation and writing – review and editing. XC: investigation, validation and writing – review and editing. ZY: resources, supervision of JD at Wuhan University of Technology, funding acquisition and writing – review and editing. AI: conceptualization, methodology, provision of the VISIT model code, supervision, funding acquisition and writing – review and editing. All authors approved the final manuscript.

Competing interests

The authors declare that they have no conflict of interest.

Acknowledgements

We acknowledge the country-specific funding of the AsiaFlux A3 Project: the National Natural Science Foundation of China (42261144688; China), the JSPS A3 Foresight Program (JPJSA3F20220002; Japan), and the National Research Foundation of Korea (NRF; No. RS-2022-NR066948; Republic of Korea).

Financial support

This study was partly supported by the Environmental and Technology Development Fund (JPMEERF21S20800) of the Environmental Restoration and Conservation Agency and the Japan Society for the Promotion of Science KAKENHI (21H05318), the National Natural Science Foundation of China (42171415), and the China Scholarship Council (202406950002).

https://doi.org/10.5194/egusphere-2026-6664
Preprint. Discussion started: 22 November 2026
© Author(s) 2026. CC BY 4.0 License.

References

Asner, G. P., Broadbent, E. N., Oliveira, P. J. C., Keller, M., Knapp, D. E., and Silva, J. N. M.: Condition and fate of logged forests in the Brazilian Amazon, Proceedings of the National Academy of Sciences, 103, 12947-12950, https://doi.org/10.1073/pnas.0604093103, 2006.

Besnard, S., Viana-Soto, A., Hartmann, H., Patacca, M., Heinrich, V. H. A., Kowalski, K., Santoro, M., De Keersmaecker, W., Van De Kerchove, R., Herold, M., and Senf, C.: Natural disturbances increasingly affect Europe's most mature and carbon-rich forests, EGUsphere, 2025, 1-27, https://doi.org/10.5194/egusphere-2025-6288, 2025.

Bourgoin, C., Ceccherini, G., Girardello, M., Vancutsem, C., Avitabile, V., Beck, P. S. A., Beuchle, R., Blanc, L., Duveiller, G., Migliavacca, M., Vieilledent, G., Cescatti, A., and Achard, F.: Human degradation of tropical moist forests is greater than previously estimated, Nature, 631, 570-576, https://doi.org/10.1038/s41586-024-07629-0, 2024.

Bousfield, C. G. and Edwards, D. P.: The pan-tropical age distribution of regenerating tropical moist forest, Nature Ecology & Evolution, 9, 1205-1213, https://doi.org/10.1038/s41559-025-02721-8, 2025.

Calle, L. and Poulter, B.: Ecosystem age-class dynamics and distribution in the LPJ-wsl v2.0 global ecosystem model, Geosci. Model Dev., 14, 2575-2601, https://doi.org/10.5194/gmd-14-2575-2021, 2021.

Chazdon, R. L., Brancalion, P. H. S., Laestadius, L., Bennett-Curry, A., Buckingham, K., Kumar, C., Moll-Rocek, J., Vieira, I. C. G., and Wilson, S. J.: When is a forest a forest? Forest concepts and definitions in the era of forest and landscape restoration, Ambio, 45, 538-550, https://doi.org/10.1007/s13280-016-0772-y, 2016.

Dong, J.: VISIT-4type v1.0: Forest age structure, wood harvest and land-cover transitions in a dynamic global vegetation model – code, input data, evaluation data and model output (1.0.2), Zenodo [code], https://doi.org/10.5281/zenodo.24367012, 2026.

Dong, J., Zhao, S., Chen, X., Yin, Z., and Ito, A.: Modeling Carbon Emissions Driven by Land-Use Change: Uncertainty and Sensitivity Analysis of Dynamic Global Vegetation Models, Global Biogeochemical Cycles, 40, e2026GB009219, https://doi.org/10.1029/2026GB009219, 2026.

Feng, Y., Zeng, Z., Searchinger, T. D., Ziegler, A. D., Wu, J., Wang, D., He, X., Elsen, P. R., Ciais, P., Xu, R., Guo, Z., Peng, L., Tao, Y., Spracklen, D. V., Holden, J., Liu, X., Zheng, Y., Xu, P., Chen, J., Jiang, X., Song, X.-P., Lakshmi, V., Wood, E. F., and Zheng, C.: Doubling of annual forest carbon loss over the tropics during the early twenty-first century, Nature Sustainability, 5, 444-451, https://doi.org/10.1038/s41893-022-00854-3, 2022.

Friedlingstein, P., O'Sullivan, M., Jones, M. W., Andrew, R. M., Bakker, D. C. E., Hauck, J., Landschützer, P., Le Quéré, C., Li, H., Luijkx, I. T., Peters, G. P., Peters, W., Pongratz, J., Schwingshackl, C., Sitch, S., Canadell, J. G., Ciais, P., Aas, K., Alin, S. R.,

https://doi.org/10.5194/egusphere-2026-6664
Preprint. Discussion started: 22 November 2026
© Author(s) 2026. CC BY 4.0 License.

Anthoni, P., Barbero, L., Bates, N. R., Bellouin, N., Benoit-Cattin, A., Berghoff, C. F., Bernardello, R., Bopp, L., Brasika, I. B. M., Chamberlain, M. A., Chandra, N., Chevallier, F., Chini, L. P., Collier, N. O., Colligan, T. H., Cronin, M., Djeutchouang, L. M., Dou, X., Enright, M. P., Enyo, K., Erb, M., Evans, W., Feely, R. A., Feng, L., Ford, D. J., Foster, A., Fransner, F., Gasser, T., Gehlen, M., Gkritzalis, T., Goncalves De Souza, J., Grassi, G., Gregor, L., Gruber, N., Guenet, B., Gürses, Ö., Harrington, K., Harris, I., Heinke, J., Hurtt, G. C., Iida, Y., Ilyina, T., Ito, A., Jacobson, A. R., Jain, A. K., Jarníková, T., Jersild, A., Jiang, F., Jones, S. D., Kato, E., Keeling, R. F., Klein Goldewijk, K., Knauer, J., Kong, Y., Korsbakken, J. I., Koven, C., Kunimitsu, T., Lan, X., Liu, J., Liu, Z., Liu, Z., Lo Monaco, C., Ma, L., Marland, G., McGuire, P. C., McKinley, G. A., Melton, J. R., Monacci, N., Monier, E., Morgan, E. J., Munro, D. R., Müller, J. D., Nakaoka, S. I., Nayagam, L. R., Niwa, Y., Nutzel, T., Olsen, A., Omar, A. M., Pan, N., Pandey, S., Pierrot, D., Qin, Z., Regnier, P., Rehder, G., Resplandy, L., Roobaert, A., Rosan, T. M., Rödenbeck, C., Schwinger, J., Skjelvan, I., Smallman, T. L., Spada, V., Sreeush, M. G., Sun, Q., Sutton, A. J., Sweeney, C., Swingedouw, D., Séférian, R., Takao, S., Tatebe, H., Tian, H., Tian, X., Tilbrook, B., Tsujino, H., Tubiello, F., van Ooijen, E., van der Werf, G. R., van de Velde, S. J., Walker, A. P., Wanninkhof, R., Yang, X., Yuan, W., Yue, X., and Zeng, J.: Global Carbon Budget 2025, Earth Syst. Sci. Data, 18, 3211-3288, https://doi.org/10.5194/essd-18-3211-2026, 2026.

Frieler, K., Volkholz, J., Lange, S., Schewe, J., Mengel, M., del Rocío Rivas López, M., Otto, C., Reyer, C. P. O., Karger, D. N., Malle, J. T., Treu, S., Menz, C., Blanchard, J. L., Harrison, C. S., Petrik, C. M., Eddy, T. D., Ortega-Cisneros, K., Novaglio, C., Rousseau, Y., Watson, R. A., Stock, C., Liu, X., Heneghan, R., Tittensor, D., Maury, O., Büchner, M., Vogt, T., Wang, T., Sun, F., Sauer, I. J., Koch, J., Vanderkelen, I., Jägermeyr, J., Müller, C., Rabin, S., Klar, J., Vega del Valle, I. D., Lasslop, G., Chadburn, S., Burke, E., Gallego-Sala, A., Smith, N., Chang, J., Hantson, S., Burton, C., Gädeke, A., Li, F., Gosling, S. N., Müller Schmied, H., Hattermann, F., Wang, J., Yao, F., Hickler, T., Marcé, R., Pierson, D., Thiery, W., Mercado-Bettín, D., Ladwig, R., Ayala-Zamora, A. I., Forrest, M., and Bechtold, M.: Scenario setup and forcing data for impact model evaluation and impact attribution within the third round of the Inter-Sectoral Impact Model Intercomparison Project (ISIMIP3a), Geosci. Model Dev., 17, 1-51, https://doi.org/10.5194/gmd-17-1-2024, 2024.

Grassi, G., Schwingshackl, C., Gasser, T., Houghton, R. A., Sitch, S., Canadell, J. G., Cescatti, A., Ciais, P., Federici, S., Friedlingstein, P., Kurz, W. A., Sanz Sanchez, M. J., Abad Viñas, R., Alkama, R., Bultan, S., Ceccherini, G., Falk, S., Kato, E., Kennedy, D., Knauer, J., Korosuo, A., Melo, J., McGrath, M. J., Nabel, J. E. M. S., Poulter, B., Romanovskaya, A. A., Rossi, S., Tian, H., Walker, A. P., Yuan, W., Yue, X., and Pongratz, J.: Harmonising the land-use flux estimates of global models and national inventories for 2000–2020, Earth Syst. Sci. Data, 15, 1093-1114, https://doi.org/10.5194/essd-15-1093-2023, 2023.

Hansis, E., Davis, S. J., and Pongratz, J.: Relevance of methodological choices for accounting of land use change carbon fluxes, Global Biogeochemical Cycles, 29, 1230-

https://doi.org/10.5194/egusphere-2026-6664
Preprint. Discussion started: 22 November 2026
© Author(s) 2026. CC BY 4.0 License.

1246, https://doi.org/10.1002/2014GB004997, 2015.

Haverd, V., Smith, B., Nieradzik, L., Briggs, P. R., Woodgate, W., Trudinger, C. M., Canadell, J. G., and Cuntz, M.: A new version of the CABLE land surface model (Subversion revision r4601) incorporating land use and land cover change, woody vegetation demography, and a novel optimisation-based approach to plant coordination of photosynthesis, Geosci. Model Dev., 11, 2995-3026, https://doi.org/10.5194/gmd-11-2995-2018, 2018.

Houghton, R. A. and Nassikas, A. A.: Global and regional fluxes of carbon from land use and land cover change 1850–2015, Global Biogeochemical Cycles, 31, 456-472, https://doi.org/10.1002/2016GB005546, 2017.

Hurtt, G. C., Chini, L., Sahajpal, R., Frolking, S., Bodirsky, B. L., Calvin, K., Doelman, J. C., Fisk, J., Fujimori, S., Klein Goldewijk, K., Hasegawa, T., Havlik, P., Heinimann, A., Humpenöder, F., Jungclaus, J., Kaplan, J. O., Kennedy, J., Krisztin, T., Lawrence, D., Lawrence, P., Ma, L., Mertz, O., Pongratz, J., Popp, A., Poulter, B., Riahi, K., Shevliakova, E., Stehfest, E., Thornton, P., Tubiello, F. N., van Vuuren, D. P., and Zhang, X.: Harmonization of global land use change and management for the period 850–2100 (LUH2) for CMIP6, Geosci. Model Dev., 13, 5425-5464, https://doi.org/10.5194/gmd-13-5425-2020, 2020.

Ito, A.: Changing ecophysiological processes and carbon budget in East Asian ecosystems under near-future changes in climate: implications for long-term monitoring from a process-based model, Journal of Plant Research, 123, 577-588, https://doi.org/10.1007/s10265-009-0305-x, 2010.

Ito, A.: Disequilibrium of terrestrial ecosystem CO2 budget caused by disturbance-induced emissions and non-CO2 carbon export flows: a global model assessment, Earth Syst. Dynam., 10, 685-709, https://doi.org/10.5194/esd-10-685-2019, 2019.

Kattge, J., Bönisch, G., Díaz, S., Lavorel, S., Prentice, I. C., Leadley, P., Tautenhahn, S., Werner, G. D. A., Aakala, T., Abedi, M., Acosta, A. T. R., Adamidis, G. C., Adamson, K., Aiba, M., Albert, C. H., Alcántara, J. M., Alcázar C, C., Aleixo, I., Ali, H., Amiaud, B., Ammer, C., Amoroso, M. M., Anand, M., Anderson, C., Anten, N., Antos, J., Apgaua, D. M. G., Ashman, T.-L., Asmara, D. H., Asner, G. P., Aspinwall, M., Atkin, O., Aubin, I., Baastrup-Spohr, L., Bahalkeh, K., Bahn, M., Baker, T., Baker, W. J., Bakker, J. P., Baldocchi, D., Baltzer, J., Banerjee, A., Baranger, A., Barlow, J., Barneche, D. R., Baruch, Z., Bastianelli, D., Battles, J., Bauerle, W., Bauters, M., Bazzato, E., Beckmann, M., Beeckman, H., Beierkuhnlein, C., Bekker, R., Belfry, G., Belluau, M., Beloiu, M., Benavides, R., Benomar, L., Berdugo-Lattke, M. L., Berenguer, E., Bergamin, R., Bergmann, J., Bergmann Carlucci, M., Berner, L., Bernhardt-Römermann, M., Bigler, C., Bjorkman, A. D., Blackman, C., Blanco, C., Blonder, B., Blumenthal, D., Bocanegra-González, K. T., Boeckx, P., Bohlman, S., Böhning-Gaese, K., Boisvert-Marsh, L., Bond, W., Bond-Lamberty, B., Boom, A., Boonman, C. C. F., Bordin, K., Boughton, E. H., Boukili, V., Bowman, D. M. J. S., Bravo, S., Brendel, M. R., Broadley, M. R., Brown, K. A., Bruelheide, H., Brumnich, F., Bruun, H. H., Bruy, D., Buchanan, S. W., Bucher, S. F., Buchmann, N., Buitenwerf,

https://doi.org/10.5194/egusphere-2026-6664
Preprint. Discussion started: 22 November 2026
© Author(s) 2026. CC BY 4.0 License.

R., Bunker, D. E., Bürger, J., Burrascano, S., Burslem, D. F. R. P., Butterfield, B. J., Byun, C., Marques, M., Scalon, M. C., Caccianiga, M., Cadotte, M., Cailleret, M., Camac, J., Camarero, J. J., Campany, C., Campetella, G., Campos, J. A., Cano-Arboleda, L., Canullo, R., Carbognani, M., Carvalho, F., Casanoves, F., Castagneyrol, B., Catford, J. A., Cavender-Bares, J., Cerabolini, B. E. L., Cervellini, M., Chacón-Madrigal, E., Chapin, K., Chapin, F. S., Chelli, S., Chen, S.-C., Chen, A., Cherubini, P., Chianucci, F., Choat, B., Chung, K.-S., Chytrý, M., Ciccarelli, D., Coll, L., Collins, C. G., Conti, L., Coomes, D., Cornelissen, J. H. C., Cornwell, W. K., Corona, P., Coyea, M., Craine, J., Craven, D., Cromsigt, J. P. G. M., Csecserits, A., Cufar, K., Cuntz, M., da Silva, A. C., Dahlin, K. M., Dainese, M., Dalke, I., Dalle Fratte, M., Dang-Le, A. T., Danihelka, J., Dannoura, M., Dawson, S., de Beer, A. J., De Frutos, A., De Long, J. R., Dechant, B., Delagrange, S., Delpierre, N., Derroire, G., Dias, A. S., Diaz-Toribio, M. H., Dimitrakopoulos, P. G., Dobrowolski, M., Doktor, D., Dřevojan, P., Dong, N., Dransfield, J., Dressler, S., Duarte, L., Ducouret, E., Dullinger, S., Durka, W., Duursma, R., Dymova, O., E-Vojtkó, A., Eckstein, R. L., Ejtehadi, H., Elser, J., Emilio, T., Engemann, K., Erfanian, M. B., Erfmeier, A., Esquivel-Muelbert, A., Esser, G., Estiarte, M., Domingues, T. F., Fagan, W. F., Fagúndez, J., Falster, D. S., Fan, Y., Fang, J., Farris, E., Fazlioglu, F., Feng, Y., Fernandez-Mendez, F., Ferrara, C., Ferreira, J., Fidelis, A., Finegan, B., Firn, J., Flowers, T. J., Flynn, D. F. B., Fontana, V., Forey, E., Forgiarini, C., François, L., Frangipani, M., Frank, D., Frenette-Dussault, C., Freschet, G. T., Fry, E. L., Fyllas, N. M., Mazzochini, G. G., Gachet, S., Gallagher, R., Ganade, G., Ganga, F., García-Palacios, P., Gargaglione, V., Garnier, E., Garrido, J. L., de Gasper, A. L., Gea-Izquierdo, G., Gibson, D., Gillison, A. N., Giroldo, A., Glasenhardt, M.-C., Gleason, S., Gliesch, M., Goldberg, E., Göldel, B., Gonzalez-Akre, E., Gonzalez-Andujar, J. L., González-Melo, A., González-Robles, A., Graae, B. J., Granda, E., Graves, S., Green, W. A., Gregor, T., Gross, N., Guerin, G. R., Günther, A., Gutiérrez, A. G., Haddock, L., Haines, A., Hall, J., Hambuckers, A., Han, W., Harrison, S. P., Hattingh, W., Hawes, J. E., He, T., He, P., Heberling, J. M., Helm, A., Hempel, S., Hentschel, J., Hérault, B., Hereş, A.-M., Herz, K., Heuertz, M., Hickler, T., Hietz, P., Higuchi, P., Hipp, A. L., Hirons, A., Hock, M., Hogan, J. A., Holl, K., Honnay, O., Hornstein, D., Hou, E., Hough-Snee, N., Hovstad, K. A., Ichie, T., Igić, B., Illa, E., Isaac, M., Ishihara, M., Ivanov, L., Ivanova, L., Iversen, C. M., Izquierdo, J., Jackson, R. B., Jackson, B., Jactel, H., Jagodzinski, A. M., Jandt, U., Jansen, S., Jenkins, T., Jentsch, A., Jespersen, J. R. P., Jiang, G.-F., Johansen, J. L., Johnson, D., Jokela, E. J., Joly, C. A., Jordan, G. J., Joseph, G. S., Junaedi, D., Junker, R. R., Justes, E., Kabzems, R., Kane, J., Kaplan, Z., Kattenborn, T., Kavelenova, L., Kearsley, E., Kempel, A., Kenzo, T., Kerkhoff, A., Khalil, M. I., Kinlock, N. L., Kissling, W. D., Kitajima, K., Kitzberger, T., Kjøller, R., Klein, T., Kleyer, M., Klimešová, J., Klipel, J., Kloeppel, B., Klotz, S., Knops, J. M. H., Kohyama, T., Koike, F., Kollmann, J., Komac, B., Komatsu, K., König, C., Kraft, N. J. B., Kramer, K., Kreft, H., Kühn, I., Kumarathunge, D., Kuppler, J., Kurokawa, H., Kurosawa, Y., Kuyah, S., Laclau, J.-P., Lafleur, B., Lallai, E., Lamb, E., Lamprecht, A., Larkin, D. J., Laughlin, D., Le Bagousse-Pinguet, Y., le

https://doi.org/10.5194/egusphere-2026-6664
Preprint. Discussion started: 22 November 2026
© Author(s) 2026. CC BY 4.0 License.

Maire, G., le Roux, P. C., le Roux, E., Lee, T., Lens, F., Lewis, S. L., Lhotsky, B., Li, Y., Li, X., Lichstein, J. W., Liebergesell, M., Lim, J. Y., Lin, Y.-S., Linares, J. C., Liu, C., Liu, D., Liu, U., Livingstone, S., Llusià, J., Lohbeck, M., López-García, Á., Lopez-Gonzalez, G., Lososová, Z., Louault, F., Lukács, B. A., Lukeš, P., Luo, Y., Lussu, M., Ma, S., Maciel Rabelo Pereira, C., Mack, M., Maire, V., Mäkelä, A., Mäkinen, H., Malhado, A. C. M., Mallik, A., Manning, P., Manzoni, S., Marchetti, Z., Marchino, L., Marcilio-Silva, V., Marcon, E., Marignani, M., Markesteijn, L., Martin, A., Martínez-Garza, C., Martínez-Vilalta, J., Mašková, T., Mason, K., Mason, N., Massad, T. J., Masse, J., Mayrose, I., McCarthy, J., McCormack, M. L., McCulloh, K., McFadden, I. R., McGill, B. J., McPartland, M. Y., Medeiros, J. S., Medlyn, B., Meerts, P., Mehrabi, Z., Meir, P., Melo, F. P. L., Mencuccini, M., Meredieu, C., Messier, J., Mészáros, I., Metsaranta, J., Michaletz, S. T., Michelaki, C., Migalina, S., Milla, R., Miller, J. E. D., Minden, V., Ming, R., Mokany, K., Moles, A. T., Molnár V, A., Molofsky, J., Molz, M., Montgomery, R. A., Monty, A., Moravcová, L., Moreno-Martínez, A., Moretti, M., Mori, A. S., Mori, S., Morris, D., Morrison, J., Mucina, L., Mueller, S., Muir, C. D., Müller, S. C., Munoz, F., Myers-Smith, I. H., Myster, R. W., Nagano, M., Naidu, S., Narayanan, A., Natesan, B., Negoita, L., Nelson, A. S., Neuschulz, E. L., Ni, J., Niedrist, G., Nieto, J., Niinemets, Ü., Nolan, R., Nottebrock, H., Nouvellon, Y., Novakovskiy, A., Network, T. N., Nystuen, K. O., O'Grady, A., O'Hara, K., O'Reilly-Nugent, A., Oakley, S., Oberhuber, W., Ohtsuka, T., Oliveira, R., Öllerer, K., Olson, M. E., Onipchenko, V., Onoda, Y., Onstein, R. E., Ordonez, J. C., Osada, N., Ostonen, I., Ottaviani, G., Otto, S., Overbeck, G. E., Ozinga, W. A., Pahl, A. T., Paine, C. E. T., Pakeman, R. J., Papageorgiou, A. C., Parfionova, E., Pärtel, M., Patacca, M., Paula, S., Paule, J., Pauli, H., Pausas, J. G., Peco, B., Penuelas, J., Perea, A., Peri, P. L., Petisco-Souza, A. C., Petraglia, A., Petritan, A. M., Phillips, O. L., Pierce, S., Pillar, V. D., Pisek, J., Pomogaybin, A., Poorter, H., Portsmuth, A., Poschlod, P., Potvin, C., Pounds, D., Powell, A. S., Power, S. A., Prinzing, A., Puglielli, G., Pyšek, P., Raevel, V., Rammig, A., Ransijn, J., Ray, C. A., Reich, P. B., Reichstein, M., Reid, D. E. B., Réjou-Méchain, M., de Dios, V. R., Ribeiro, S., Richardson, S., Riibak, K., Rillig, M. C., Riviera, F., Robert, E. M. R., Roberts, S., Robroek, B., Roddy, A., Rodrigues, A. V., Rogers, A., Rollinson, E., Rolo, V., Römermann, C., Ronzhina, D., Roscher, C., Rosell, J. A., Rosenfield, M. F., Rossi, C., Roy, D. B., Royer-Tardif, S., Rüger, N., Ruiz-Peinado, R., Rumpf, S. B., Rusch, G. M., Ryo, M., Sack, L., Saldaña, A., Salgado-Negret, B., Salguero-Gomez, R., Santa-Regina, I., Santacruz-García, A. C., Santos, J., Sardans, J., Schamp, B., Scherer-Lorenzen, M., Schleuning, M., Schmid, B., Schmidt, M., Schmitt, S., Schneider, J. V., Schowanek, S. D., Schrader, J., Schrodt, F., Schuldt, B., Schurr, F., Selaya Garvizu, G., Semchenko, M., Seymour, C., Sfair, J. C., Sharpe, J. M., Sheppard, C. S., Sheremetiev, S., Shiodera, S., Shipley, B., Shovon, T. A., Siebenkäs, A., Sierra, C., Silva, V., Silva, M., Sitzia, T., Sjöman, H., Slot, M., Smith, N. G., Sodhi, D., Soltis, P., Soltis, D., Somers, B., Sonnier, G., Sørensen, M. V., Sosinski Jr, E. E., Soudzilovskaia, N. A., Souza, A. F., Spasojevic, M., Sperandii, M. G., Stan, A. B., Stegen, J., Steinbauer, K., Stephan, J. G., Sterck, F., Stojanovic, D. B., Strydom, T.,

https://doi.org/10.5194/egusphere-2026-6664
Preprint. Discussion started: 22 November 2026
© Author(s) 2026. CC BY 4.0 License.

Suarez, M. L., Svenning, J.-C., Svitková, I., Svitok, M., Svoboda, M., Swaine, E., Swenson, N., Tabarelli, M., Takagi, K., Tappeiner, U., Tarifa, R., Tauugourdeau, S., Tavsanoglu, C., te Beest, M., Tedersoo, L., Thiffault, N., Thom, D., Thomas, E., Thompson, K., Thornton, P. E., Thuiller, W., Tichý, L., Tissue, D., Tjoelker, M. G., Tng, D. Y. P., Tobias, J., Török, P., Tarin, T., Torres-Ruiz, J. M., Tóthmérész, B., Treurnicht, M., Trivellone, V., Trolliet, F., Trotsiuk, V., Tsakalos, J. L., Tsiripidis, I., Tysklind, N., Umehara, T., Usoltsev, V., Vadeboncoeur, M., Vaezi, J., Valladares, F., Vamosi, J., van Bodegom, P. M., van Breugel, M., Van Cleemput, E., van de Weg, M., van der Merwe, S., van der Plas, F., van der Sande, M. T., van Kleunen, M., Van Meerbeek, K., Vanderwel, M., Vanselow, K. A., Vårhammar, A., Varone, L., Vasquez Valderrama, M. Y., Vassilev, K., Vellend, M., Veneklaas, E. J., Verbeeck, H., Verheyen, K., Vibrans, A., Vieira, I., Villacís, J., Violle, C., Vivek, P., Wagner, K., Waldram, M., Waldron, A., Walker, A. P., Waller, M., Walther, G., Wang, H., Wang, F., Wang, W., Watkins, H., Watkins, J., Weber, U., Weedon, J. T., Wei, L., Weigelt, P., Weiher, E., Wells, A. W., Wellstein, C., Wenk, E., Westoby, M., Westwood, A., White, P. J., Whitten, M., Williams, M., Winkler, D. E., Winter, K., Womack, C., Wright, I. J., Wright, S. J., Wright, J., Pinho, B. X., Ximenes, F., Yamada, T., Yamaji, K., Yanai, R., Yankov, N., Yguel, B., Zanini, K. J., Zanne, A. E., Zelený, D., Zhao, Y.-P., Zheng, J., Zheng, J., Ziemińska, K., Zirbel, C. R., Zizka, G., Zo-Bi, I. C., Zotz, G., and Wirth, C.: TRY plant trait database – enhanced coverage and open access, Global Change Biology, 26, 119-188, https://doi.org/10.1111/gcb.14904, 2020.

Lange, S., Mengel, M., Treu, S., and Büchner, M.: ISIMIP3a atmospheric climate input data (v1.0), ISIMIP Repository [data set], https://doi.org/10.48364/ISIMIP.982724, 2022.

Li, W., Yue, C., Ciais, P., Chang, J., Goll, D., Zhu, D., Peng, S., and Jornet-Puig, A.: ORCHIDEE-MICT-BIOENERGY: an attempt to represent the production of lignocellulosic crops for bioenergy in a global vegetation model, Geosci. Model Dev., 11, 2249-2272, https://doi.org/10.5194/gmd-11-2249-2018, 2018.

Lindeskog, M., Smith, B., Lagergren, F., Sycheva, E., Ficko, A., Pretzsch, H., and Rammig, A.: Accounting for forest management in the estimation of forest carbon balance using the dynamic vegetation model LPJ-GUESS (v4.0, r9710): implementation and evaluation of simulations for Europe, Geosci. Model Dev., 14, 6071-6112, https://doi.org/10.5194/gmd-14-6071-2021, 2021.

Ma, L., Hurtt, G. C., Chini, L. P., Sahajpal, R., Pongratz, J., Frolking, S., Stehfest, E., Klein Goldewijk, K., O'Leary, D., and Doelman, J. C.: Global rules for translating land-use change (LUH2) to land-cover change for CMIP6 using GLM2, Geosci. Model Dev., 13, 3203-3220, https://doi.org/10.5194/gmd-13-3203-2020, 2020.

Mason Earles, J., Yeh, S., and Skog, K. E.: Timing of carbon emissions from global forest clearance, Nature Climate Change, 2, 682-685, https://doi.org/10.1038/nclimate1535, 2012.

McGuire, A. D., Sitch, S., Clein, J. S., Dargaville, R., Esser, G., Foley, J., Heimann, M., Joos, F., Kaplan, J., Kicklighter, D. W., Meier, R. A., Melillo, J. M., Moore III, B.,

https://doi.org/10.5194/egusphere-2026-6664
Preprint. Discussion started: 22 November 2026
© Author(s) 2026. CC BY 4.0 License.

Prentice, I. C., Ramankutty, N., Reichenau, T., Schloss, A., Tian, H., Williams, L. J., and Wittenberg, U.: Carbon balance of the terrestrial biosphere in the Twentieth Century: Analyses of CO2, climate and land use effects with four process-based ecosystem models, Global Biogeochemical Cycles, 15, 183-206, https://doi.org/10.1029/2000GB001298, 2001.

Nelson, J. A., Walther, S., Gans, F., Kraft, B., Weber, U., Novick, K., Buchmann, N., Migliavacca, M., Wohlfahrt, G., Šigut, L., Ibrom, A., Papale, D., Göckede, M., Duveiller, G., Knohl, A., Hörtnagl, L., Scott, R. L., Dušek, J., Zhang, W., Hamdi, Z. M., Reichstein, M., Aranda-Barranco, S., Ardö, J., Op de Beeck, M., Billesbach, D., Bowling, D., Bracho, R., Brümmer, C., Camps-Valls, G., Chen, S., Cleverly, J. R., Desai, A., Dong, G., El-Madany, T. S., Euskirchen, E. S., Feigenwinter, I., Galvagno, M., Gerosa, G. A., Gielen, B., Goded, I., Goslee, S., Gough, C. M., Heinesch, B., Ichii, K., Jackowicz-Korczynski, M. A., Klosterhalfen, A., Knox, S., Kobayashi, H., Kohonen, K. M., Korkiakoski, M., Mammarella, I., Gharun, M., Marzuoli, R., Matamala, R., Metzger, S., Montagnani, L., Nicolini, G., O'Halloran, T., Ourcival, J. M., Peichl, M., Pendall, E., Ruiz Reverter, B., Roland, M., Sabbatini, S., Sachs, T., Schmidt, M., Schwalm, C. R., Shekhar, A., Silberstein, R., Silveira, M. L., Spano, D., Tagesson, T., Tramontana, G., Trotta, C., Turco, F., Vesala, T., Vincke, C., Vitale, D., Vivoni, E. R., Wang, Y., Woodgate, W., Yepez, E. A., Zhang, J., Zona, D., and Jung, M.: X-BASE: the first terrestrial carbon and water flux products from an extended data-driven scaling framework, FLUXCOM-X, Biogeosciences, 21, 5079-5115, https://doi.org/10.5194/bg-21-5079-2024, 2024.

Olson, J. S., Watts, J. A., and Allison, L. J.: Carbon in live vegetation of major world ecosystems, Report ORNL-5862, Oak Ridge National Laboratory, Oak Ridge, Tennessee, USA, https://hero.epa.gov/reference/3230285/, 1983.

Pan, Y., Birdsey, R. A., Fang, J., Houghton, R., Kauppi, P. E., Kurz, W. A., Phillips, O. L., Shvidenko, A., Lewis, S. L., Canadell, J. G., Ciais, P., Jackson, R. B., Pacala, S. W., McGuire, A. D., Piao, S., Rautiainen, A., Sitch, S., and Hayes, D.: A Large and Persistent Carbon Sink in the World's Forests, Science, 333, 988-993, https://doi.org/10.1126/science.1201609, 2011.

Pastorello, G., Trotta, C., Canfora, E., Chu, H., Christianson, D., Cheah, Y.-W., Poindexter, C., Chen, J., Elbashandy, A., Humphrey, M., Isaac, P., Polidori, D., Reichstein, M., Ribeca, A., van Ingen, C., Vuichard, N., Zhang, L., Amiro, B., Ammann, C., Arain, M. A., Ardö, J., Arkebauer, T., Arndt, S. K., Arriga, N., Aubinet, M., Aurela, M., Baldocchi, D., Barr, A., Beamesderfer, E., Marchesini, L. B., Bergeron, O., Beringer, J., Bernhofer, C., Berveiller, D., Billesbach, D., Black, T. A., Blanken, P. D., Bohrer, G., Boike, J., Bolstad, P. V., Bonal, D., Bonnefond, J.-M., Bowling, D. R., Bracho, R., Brodeur, J., Brümmer, C., Buchmann, N., Burban, B., Burns, S. P., Buysse, P., Cale, P., Cavagna, M., Cellier, P., Chen, S., Chini, I., Christensen, T. R., Cleverly, J., Collalti, A., Consalvo, C., Cook, B. D., Cook, D., Coursolle, C., Cremonese, E., Curtis, P. S., D'Andrea, E., da Rocha, H., Dai, X., Davis, K. J., Cinti, B. D., Grandcourt, A. d., Ligne, A. D., De Oliveira, R. C., Delpierre, N., Desai, A. R., Di Bella, C. M., Tommasi,

https://doi.org/10.5194/egusphere-2026-6664
Preprint. Discussion started: 22 November 2026
© Author(s) 2026. CC BY 4.0 License.

P. d., Dolman, H., Domingo, F., Dong, G., Dore, S., Duce, P., Dufrêne, E., Dunn, A., Dušek, J., Eamus, D., Eichelmann, U., ElKhidir, H. A. M., Eugster, W., Ewenz, C. M., Ewers, B., Famulari, D., Fares, S., Feigenwinter, I., Feitz, A., Fensholt, R., Filippa, G., Fischer, M., Frank, J., Galvagno, M., Gharun, M., Gianelle, D., Gielen, B., Gioli, B., Gitelson, A., Goded, I., Goeckede, M., Goldstein, A. H., Gough, C. M., Goulden, M. L., Graf, A., Griebel, A., Gruening, C., Grünwald, T., Hammerle, A., Han, S., Han, X., Hansen, B. U., Hanson, C., Hatakka, J., He, Y., Hehn, M., Heinesch, B., Hinko-Najera, N., Hörtnagl, L., Hutley, L., Ibrom, A., Ikawa, H., Jackowicz-Korczynski, M., Janouš, D., Jans, W., Jassal, R., Jiang, S., Kato, T., Khomik, M., Klatt, J., Knohl, A., Knox, S., Kobayashi, H., Koerber, G., Kolle, O., Kosugi, Y., Kotani, A., Kowalski, A., Kruijt, B., Kurbatova, J., Kutsch, W. L., Kwon, H., Launiainen, S., Laurila, T., Law, B., Leuning, R., Li, Y., Liddell, M., Limousin, J.-M., Lion, M., Liska, A. J., Lohila, A., López-Ballesteros, A., López-Blanco, E., Loubet, B., Loustau, D., Lucas-Moffat, A., Lüers, J., Ma, S., Macfarlane, C., Magliulo, V., Maier, R., Mammarella, I., Manca, G., Marcolla, B., Margolis, H. A., Marras, S., Massman, W., Mastepanov, M., Matamala, R., Matthes, J. H., Mazzenga, F., McCaughey, H., McHugh, I., McMillan, A. M. S., Merbold, L., Meyer, W., Meyers, T., Miller, S. D., Minerbi, S., Moderow, U., Monson, R. K., Montagnani, L., Moore, C. E., Moors, E., Moreaux, V., Moureaux, C., Munger, J. W., Nakai, T., Neirynck, J., Nesic, Z., Nicolini, G., Noormets, A., Northwood, M., Nosetto, M., Nouvellon, Y., Novick, K., Oechel, W., Olesen, J. E., Ourcival, J.-M., Papuga, S. A., Parmentier, F.-J., Paul-Limoges, E., Pavelka, M., Peichl, M., Pendall, E., Phillips, R. P., Pilegaard, K., Pirk, N., Posse, G., Powell, T., Prasse, H., Prober, S. M., Rambal, S., Rannik, Ü., Raz-Yaseef, N., Rebmann, C., Reed, D., Dios, V. R. d., Restrepo-Coupe, N., Reverter, B. R., Roland, M., Sabbatini, S., Sachs, T., Saleska, S. R., Sánchez-Cañete, E. P., Sanchez-Mejia, Z. M., Schmid, H. P., Schmidt, M., Schneider, K., Schrader, F., Schroder, I., Scott, R. L., Sedlák, P., Serrano-Ortíz, P., Shao, C., Shi, P., Shironya, I., Siebicke, L., Šigut, L., Silberstein, R., Sirca, C., Spano, D., Steinbrecher, R., Stevens, R. M., Sturtevant, C., Suyker, A., Tagesson, T., Takanashi, S., Tang, Y., Tapper, N., Thom, J., Tomassucci, M., Tuovinen, J.-P., Urbanski, S., Valentini, R., van der Molen, M., van Gorsel, E., van Huissteden, K., Varlagin, A., Verfaillie, J., Vesala, T., Vincke, C., Vitale, D., Vygodskaya, N., Walker, J. P., Walter-Shea, E., Wang, H., Weber, R., Westermann, S., Wille, C., Wofsy, S., Wohlfahrt, G., Wolf, S., Woodgate, W., Li, Y., Zampedri, R., Zhang, J., Zhou, G., Zona, D., Agarwal, D., Biraud, S., Torn, M., and Papale, D.: The FLUXNET2015 dataset and the ONEFlux processing pipeline for eddy covariance data, Scientific Data, 7, 225, https://doi.org/10.1038/s41597-020-0534-3, 2020.

Peng, L., Searchinger, T. D., Zionts, J., and Waite, R.: The carbon costs of global wood harvests, Nature, 620, 110-115, https://doi.org/10.1038/s41586-023-06187-1, 2023.

Pongratz, J., Reick, C. H., Houghton, R. A., and House, J. I.: Terminology as a key uncertainty in net land use and land cover change carbon flux estimates, Earth Syst. Dynam., 5, 177-195, https://doi.org/10.5194/esd-5-177-2014, 2014.

https://doi.org/10.5194/egusphere-2026-6664
Preprint. Discussion started: 22 November 2026
© Author(s) 2026. CC BY 4.0 License.

Poorter, L. and Bongers, F.: Leaf traits are good predictors of plant performance across 53 rain forest species, Ecology, 87, 1733-1743, https://doi.org/10.1890/0012-9658(2006)87[1733:LTAGPO]2.0.CO;2, 2006.

Poorter, L., Rozendaal, D. M. A., Bongers, F., Almeida, J. S., Álvarez, F. S., Andrade, J. L., Arreola Villa, L. F., Becknell, J. M., Bhaskar, R., Boukili, V., Brancalion, P. H. S., César, R. G., Chave, J., Chazdon, R. L., Dalla Colletta, G., Craven, D., de Jong, B. H. J., Denslow, J. S., Dent, D. H., DeWalt, S. J., Díaz García, E., Dupuy, J. M., Durán, S. M., Espírito Santo, M. M., Fernandes, G. W., Finegan, B., Granda Moser, V., Hall, J. S., Hernández-Stefanoni, J. L., Jakovac, C. C., Kennard, D., Lebrija-Trejos, E., Letcher, S. G., Lohbeck, M., Lopez, O. R., Marín-Spiotta, E., Martínez-Ramos, M., Meave, J. A., Mora, F., de Souza Moreno, V., Müller, S. C., Muñoz, R., Muscarella, R., Nunes, Y. R. F., Ochoa-Gaona, S., Oliveira, R. S., Paz, H., Sanchez-Azofeifa, A., Sanaphre-Villanueva, L., Toledo, M., Uriarte, M., Utrera, L. P., van Breugel, M., van der Sande, M. T., Veloso, M. D. M., Wright, S. J., Zanini, K. J., Zimmerman, J. K., and Westoby, M.: Functional recovery of secondary tropical forests, Proceedings of the National Academy of Sciences, 118, e2003405118, https://doi.org/10.1073/pnas.2003405118, 2021.

Poorter, L., Bongers, F., Aide, T. M., Almeyda Zambrano, A. M., Balvanera, P., Becknell, J. M., Boukili, V., Brancalion, P. H., Broadbent, E. N., Chazdon, R. L., Craven, D., de Almeida-Cortez, J. S., Cabral, G. A., de Jong, B. H., Denslow, J. S., Dent, D. H., DeWalt, S. J., Dupuy, J. M., Durán, S. M., Espírito-Santo, M. M., Fandino, M. C., César, R. G., Hall, J. S., Hernandez-Stefanoni, J. L., Jakovac, C. C., Junqueira, A. B., Kennard, D., Letcher, S. G., Licona, J. C., Lohbeck, M., Marín-Spiotta, E., Martínez-Ramos, M., Massoca, P., Meave, J. A., Mesquita, R., Mora, F., Muñoz, R., Muscarella, R., Nunes, Y. R., Ochoa-Gaona, S., de Oliveira, A. A., Orihuela-Belmonte, E., Peña-Claros, M., Pérez-García, E. A., Piotto, D., Powers, J. S., Rodríguez-Velázquez, J., Romero-Pérez, I. E., Ruíz, J., Saldarriaga, J. G., Sanchez-Azofeifa, A., Schwartz, N. B., Steininger, M. K., Swenson, N. G., Toledo, M., Uriarte, M., van Breugel, M., van der Wal, H., Veloso, M. D., Vester, H. F., Vicentini, A., Vieira, I. C., Bentos, T. V., Williamson, G. B., and Rozendaal, D. M.: Biomass resilience of Neotropical secondary forests, Nature, 530, 211-214, https://doi.org/10.1038/nature16512, 2016.

Pugh, T. A. M., Lindeskog, M., Smith, B., Poulter, B., Arneth, A., Haverd, V., and Calle, L.: Role of forest regrowth in global carbon sink dynamics, Proceedings of the National Academy of Sciences, 116, 4382-4387, https://doi.org/10.1073/pnas.1810512116, 2019.

Ramankutty, N. and Foley, J. A.: Estimating historical changes in global land cover: Croplands from 1700 to 1992, Global Biogeochemical Cycles, 13, 997-1027, https://doi.org/10.1029/1999GB900046, 1999.

Shevliakova, E., Pacala, S. W., Malyshev, S., Hurtt, G. C., Milly, P. C. D., Caspersen, J. P., Sentman, L. T., Fisk, J. P., Wirth, C., and Crevoisier, C.: Carbon cycling under 300 years of land use change: Importance of the secondary vegetation sink, Global Biogeochemical Cycles, 23, https://doi.org/10.1029/2007GB003176, 2009.

https://doi.org/10.5194/egusphere-2026-6664
Preprint. Discussion started: 22 November 2026
© Author(s) 2026. CC BY 4.0 License.

Sitch, S., O'Sullivan, M., Robertson, E., Friedlingstein, P., Albergel, C., Anthoni, P., Arneth, A., Arora, V. K., Bastos, A., Bastrikov, V., Bellouin, N., Canadell, J. G., Chini, L., Ciais, P., Falk, S., Harris, I., Hurtt, G., Ito, A., Jain, A. K., Jones, M. W., Joos, F., Kato, E., Kennedy, D., Klein Goldewijk, K., Kluzek, E., Knauer, J., Lawrence, P. J., Lombardozzi, D., Melton, J. R., Nabel, J. E. M. S., Pan, N., Peylin, P., Pongratz, J., Poulter, B., Rosan, T. M., Sun, Q., Tian, H., Walker, A. P., Weber, U., Yuan, W., Yue, X., and Zaehle, S.: Trends and Drivers of Terrestrial Sources and Sinks of Carbon Dioxide: An Overview of the TRENDY Project, Global Biogeochemical Cycles, 38, e2024GB008102, https://doi.org/10.1029/2024GB008102, 2024.

Ueyama, M., Takao, Y., Yazawa, H., Tanaka, M., Yabuki, H., Kumagai, T., Iwata, H., Awal, M. A., Du, M., Harazono, Y., Hata, Y., Hirano, T., Hiura, T., Ide, R., Ishida, S., Ishikawa, M., Kitamura, K., Kominami, Y., Komiya, S., Kotani, A., Inoue, Y., Machimura, T., Matsumoto, K., Matsuura, Y., Mizoguchi, Y., Murayama, S., Nagano, H., Nakai, T., Nakaji, T., Nakaya, K., Ohkubo, S., Ohta, T., Ono, K., Saitoh, T. M., Sakabe, A., Shimizu, T., Shimoda, S., Sugita, M., Takagi, K., Takahashi, Y., Takamura, N., Takanashi, S., Takimoto, T., Yasuda, Y., Wang, Q., Asanuma, J., Hasegawa, H., Hiyama, T., Iijima, Y., Ishidoya, S., Itoh, M., Kato, T., Kondo, H., Kosugi, Y., Kume, T., Maeda, T., Matsuura, S., Maximov, T., Miyama, T., Moriwaki, R., Muraoka, H., Petrov, R., Suzuki, J., Taniguchi, S., and Ichii, K.: The JapanFlux2024 dataset for eddy covariance observations covering Japan and East Asia from 1990 to 2023, Earth Syst. Sci. Data, 17, 3807-3833, https://doi.org/10.5194/essd-17-3807-2025, 2025.

Volkholz, J. and Ostberg, S.: ISIMIP3a N-fertilizer input data (v1.0), ISIMIP Repository [data set], https://doi.org/10.48364/ISIMIP.311496, 2020.

Wilkenskjeld, S., Kloster, S., Pongratz, J., Raddatz, T., and Reick, C. H.: Comparing the influence of net and gross anthropogenic land-use and land-cover changes on the carbon cycle in the MPI-ESM, Biogeosciences, 11, 4817-4828, https://doi.org/10.5194/bg-11-4817-2014, 2014.

Yang, J. and Tian, H.: ISIMIP3a N-deposition input data (v1.0), ISIMIP Repository [data set], https://doi.org/10.48364/ISIMIP.759077, 2020.

Yue, C., Ciais, P., and Li, W.: Smaller global and regional carbon emissions from gross land use change when considering sub-grid secondary land cohorts in a global dynamic vegetation model, Biogeosciences, 15, 1185-1201, https://doi.org/10.5194/bg-15-1185-2018, 2018a.

Yue, C., Ciais, P., Luyssaert, S., Li, W., McGrath, M. J., Chang, J., and Peng, S.: Representing anthropogenic gross land use change, wood harvest, and forest age dynamics in a global vegetation model ORCHIDEE-MICT v8.4.2, Geosci. Model Dev., 11, 409-428, https://doi.org/10.5194/gmd-11-409-2018, 2018b.